Final Report

Point Loma Ocean Outfall Plume Behavior Study

Prepared For

City of San Diego Public Utilities Department

NOAA Award No. NA08NOS4730441
(UCSD Contract H094679)

Prepared By

Scripps Institution of Oceanography
University of California, San Diego
9500 Gilman Drive
La Jolla, CA 92093-0213

Principal Contact	Peter Rogowski, Postdoctoral Researcher
Principal Investigators	P. Edward Parnell, Associate Researcher Paul Dayton, Professor Eric Terrill, CORDC Director

September 14, 2012

Updated 11/14/12, T.D. Stebbins
(tstebbins@sandiego.gov)

Point Loma Ocean Outfall Plume Behavior Study

Peter Rogowski*, Eric Terrill, Mark Otero, Lisa Hazard, Sung Yong Kim
Coastal Observing Research and Development Center (CORDC)
Marine Physical Laboratory
Scripps Institution of Oceanography

P. Edward Parnell, Paul Dayton
Coastal Ecology Group
Integrative Oceanography Division
Scripps Institution of Oceanography

**lead author*

EXECUTIVE SUMMARY

The discharge of municipal wastewater into natural environments poses potential risks to ecosystems, public health, and the beneficial uses of these environments by humans. The practice of wastewater disposal into coastal environments in the U.S. has advanced tremendously over the last half century from discharging untreated or partly treated sewage effluent in shallow water close to shore (even within bays and estuaries) to the discharge of highly treated effluent through deep ocean outfalls engineered to achieve rapid dilution and prevent the wastewater plumes from surfacing. Surfacing wastewater plumes pose increased risks to public health and to beneficial uses because they are more likely to contact the shoreline due to the typical pattern of daily onshore wind that is ubiquitous along coastlines worldwide. Most modern deep ocean outfalls achieve high rates of dilution and subsurface trapping by discharging through multiple diffuser ports distributed along long diffusers which are situated well below the oceanic thermocline which acts as a cap for the buoyant rising plume. Risk management of wastewater discharge is an evolving science that advances through the interplay of observation, monitoring, and engineering refinement. The present study focused on observation and monitoring of the Point Loma Ocean Outfall (PLOO), operated by the City of San Diego, to gauge its performance and to inform ongoing biological, sediment and water quality monitoring programs.

Specifically, we report the results of a study funded by an award to the City of San Diego by the National Oceanographic and Atmospheric Administration (NOAA Award No. NA08NOS4730441) that was designed to determine the characteristic fates of the wastewater plume emanating from the City's Point Loma Ocean Outfall (PLOO). The study focused on describing the physical oceanographic environment into which wastewater is discharged via the outfall and how that environment interacts with the resultant wastewater plume. This interaction determines how much the plume is diluted as it rises in the water column and mixes turbulently with ambient seawater, how high the plume rises, where the plume is

transported, and how quickly the plume is further diluted as it is transported downfield by currents. Thus, this study both informs on the performance of the Pt. Loma outfall as well as serves to identify specific areas of the coastal shelf off San Diego that are most likely to be affected by PLOO wastewater.

The study consisted of a combination of observational and modeling approaches. The observational component included observations of ocean currents and temperature intended to characterize the current and temperature structure of receiving ocean waters on the Pt. Loma shelf and to support of the use of an autonomous underwater vehicle (AUV) equipped with sensors capable of detecting the plume. The modeling component consisted of predicting plume rise height in the near field and post-hoc validation with AUV based observations of plume dilution.

Plume detection was facilitated using an optical sensor on the AUV that enabled the estimation of colored dissolved organic matter (CDOM). CDOM occurs naturally but exists in much greater concentrations in wastewater and thus serves as a useful tracer of wastefield dispersion in coastal environments. Ocean temperatures and currents estimated directly over the outfall discharge area and made available in real time via telemetry to shore, were used to pre-program the AUV to navigate the likely trajectory (horizontal movement and vertical position within the water column) given current and temperature structure. Upon deployment, the AUV navigated programmed tracklines oscillating in depth between the near-surface and several meters below the estimated trapping depth of the plume. Current meters were also deployed in shallower waters along the 35 m contour to resolve the most likely areas affected by wastewater plume incursion closer to shore.

The results of the study indicated that the PLOO wastefield never surfaced, and its shallowest depth during the observational period was 35 m. Further, given the hydrographic conditions of Pt. Loma shelf waters and the discharge characteristics of the outfall, the probability of the plume surfacing is highly unlikely. Observed rise heights were consistently less than modeled predictions indicating that the application of existing models to the PLOO overestimate the rise height by ~20%. This indicates that the PLOO performs better than predicted with respect to subsurface plume trapping. However, dilution rates were less than predicted since the greatest dilution rates occur as the plume rises. This was observationally confirmed as dilutions were typically 60-80% of prediction. Design parameters such as port spacing were likely the cause of these deviations from modeled predictions. Most importantly, we observed that the plume was advected mainly alongshore with only two instances where the plume moved toward shore but shoaled in waters deeper than the kelp forest (~30 m). Inshore current observations indicate that upwelling circulation, of tidal period or longer, are mostly associated with southeastward movement of the plume. The implication of this is that given the most likely plume shoaling conditions the PLOO wastefield is typically directed away from Pt. Loma and the kelp forest.

We also conclude that our hydrographic observations of currents and temperature at the outfall discharge site enabled adequate estimation of plume trajectory. Therefore, hydrographic observations alone are adequate to predict PLOO plume behavior. The most likely areas of shelf waters and sediments affected by the plume are oriented NNW to SSE as currents mainly alternate between these two directions. The plume was observed to extend

for more than 9 km from the diffusers in these dominant directions during several monitoring missions.

As a result of our findings, we propose the following recommendations to enhance and refine future receiving waters monitoring efforts for the PLOO discharge region.

Recommendation 1: Operation of a permanent oceanographic mooring system located near the terminal diffuser wye structure of the outfall (discharge site) designed to measure subsurface velocity and ocean stratification should be continued to document the state of the receiving waters into which the PLOO discharges.

Recommendation 2: The quarterly water quality sampling component of the City's ocean monitoring program for the PLOO region should be modified to use telemetered current meter/temperature data from a permanent mooring (see Rec 1) located near the outfall discharge site to design a more adaptive and optimized sampling grid pattern for each survey.

Recommendation 3: In order to measure plume location and dilution levels most effectively, operation of a mobile AUV as described herein should be in place and integrated with near-real-time reports of water column stratification and subsurface velocity.

Contents

List of Tables

List of Figures

I. INTRODUCTION

The Point Loma Ocean Outfall (PLOO) discharges an average of ~160 million gallons (~0.7 km^3) per day of treated sewage from the Point Loma Wastewater Treatment Plant (PLWTP) into the coastal shelf waters off San Diego. The effluent is treated to a level of advanced primary, wherein at least 85% of suspended solids are removed before being discharged into the Pacific Ocean through a diffusive outfall located ~7.2 km offshore of Point Loma in waters ~100 m deep. At the outset of our study, the behavior of the PLOO wastewater plume (wastefield) was not well known because it had not been studied with the necessary tools to map its three-dimensional extent in a Lagrangian manner over the time and space scales of initial and far-field secondary dilution. The behavior and spatial extent of ocean wastefields off San Diego are complex given the dynamic and complex ocean conditions on the San Diego shelf. Ocean conditions that affect plume behavior off San Diego are known to vary seasonally and are affected by larger scale ocean circulation within the southern California borderlands, local wind patterns, and winds located as far south as southern Baja California.

The purpose of the work presented here was to determine the behavior and dispersion of the PLOO plume using state-of-the-art methodology and equipment. The goals of our project are to address two primary concerns of operating the ocean outfall in its current configuration: (1) possible effects to beach and near-surface water quality and (2) its risk to the coastal marine environment. This study addresses beach and surface water quality concerns by determining whether the wastewater plume surfaces and encroaches upon beaches, and if so, to estimate the frequency of such events. It also supports efforts to address ecosystem concerns by determining the frequency of spatial occurrence (i.e. the temporal footprint) of the plume thereby helping to spatially focus current and future biological and water and sediment quality monitoring programs.

The work outlined here involved (1) tracking the wastefield using an autonomous underwater vehicle (AUV) whose daily track was based on telemetered buoy observations of currents and temperature structure at the end of the outfall, (2) modeling near-field plume behavior off Point Loma, and (3) observations of inner shelf bottom temperature and currents just offshore of the kelp forests using acoustic current profilers.

Information from these three major components supported the description of plume behavior across a broad spectrum of ocean conditions. The modeling effort consisted of using an EPA standard near-field model that describes the footprint, mixing and rising of the buoyant plume. The nearshore current meter and temperature data collected just offshore of the kelp forest provided information on the directionality of nearshore currents during upwelling events when conditions are most favorable for transporting the submerged wastefield into the kelp forest. Ocean circulation and temperature observations were conducted from December 2009 to February of 2012. AUV deployments were conducted from April 2010 to May 2011.

II. METHODS

A. Description of Study Area

The study area (Figure 1) is centered around the Y-shaped outfall that terminates in two 760 m diffuser legs oriented at an internal angle of roughly 151.5 degrees. The average volume of effluent discharged between 93 and 95 m is ~7.89 m^3/s. The bottom topography from the shore at Point Loma to the outfall discharge zone gently slopes to approximately 100 m. Beyond the 100 m isobaths there is a complex network of submarine canyons which make up the La Jolla Canyon Channel system. The currents in the region experience a variety of local driving mechanisms including barotropic tides, internal tides, and winds, as well as larger scale flows such as the seasonally northward flowing Davidson countercurrent and the

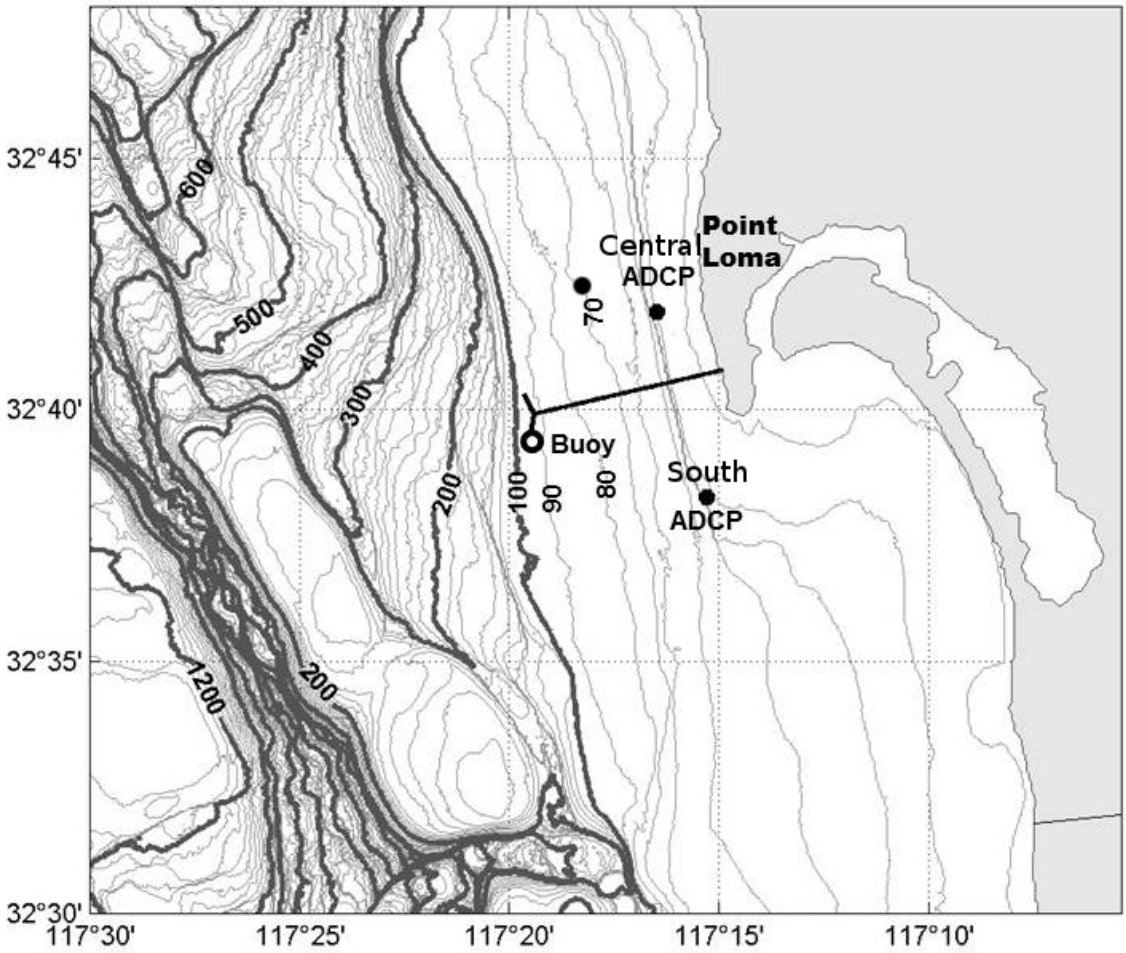

Figure 1. Location of the Point Loma Ocean Outfall (PLOO), the nearshore ADCP's and telemetered monitoring mooring (buoy).

southward flowing California Current. Tides are governed by a mixed diurnal-semidiurnal tidal forcing, with a dominant semidiurnal component [*Chadwick and Largier*, 1999].

The submarine topography associated with the Point Loma headland complicates the local current flow. The mean current direction adjacent to Point Loma is southward with typical alongshore flow speeds of 5 – 20 cm/s. As the water continues southward past the headland it separates from the coast and a vorticity maximum is observed west of Point Loma. The flow diverges from the coast at the tip of the headland, leading to upwelling of cold nutrient-rich deeper waters [*Hendricks and Christensen*, 1987, *Roughan et al., 2005*].

The seasonality of southern California is responsible for the stratification patterns of the local waters. Warmer waters and a more stratified ocean typically are present during the dry season (April through September), with the warmest temperatures occurring in August and September. Cooler waters and weak stratification characterize the ocean conditions during the wet season (October thorough March) [*Terrill*, 2009]. Typical stratification depths range between 30 - 40 m. Below these depths minimal variability in stratification depth is observed throughout the year.

The circulation feature most likely to transport the submerged wastefield emanating from the PLOO towards shore is the onshore progression of the internal tide. The internal tide propagates along the thermocline and is strongest during spring tidal conditions. The shoreward progression of the internal tide manifests as onshore currents predominating at subthermocline depths where the submerged wastefield is most likely trapped. The nearshore ADCP observations were thereby needed to determine the behavior of the internal tide over the inner shelf nearer the kelp forests and beaches.

B. Current and Temperature Observations

1. Telemetry Mooring

An oceanographic buoy designed and built by Scripps Institution of Oceanography for real-time monitoring of ocean conditions at POTW outfalls was used for this study. The mooring consisted of a surface buoy that contained an Acoustic Doppler Current Profiler (ADCP, TRDI Instruments, San Diego, CA) a temperature chain (Precision Measurement Engineering, Encinitas, CA), data logger, satellite telemetry unit, Global Positioning System (GPS) receiver, and a battery pack. The downward looking ADCP profiled ocean currents from 4.3 m deep to the seafloor. All mechanical aspects of the buoy, mooring, and anchoring system were fabricated by Scripps (Figures 2 and 3).

The system was designed for a nominal 6-month servicing interval to replace sensor batteries and offload data from the internal memory recorders. Due to mechanical wear and fatigue on the mooring components, major components of the mooring (swivels, chain, and shackles) were also replaced at this time.

Ocean currents were measured using the ADCP. The ADCP estimates currents by transmitting pulses of sound through the water column and measuring the Doppler shift of the signal scattered from particles moving with the ocean currents. The ADCP was oriented to be downward looking from the surface buoy and provides a profile of ocean currents from 4.3 m to the seafloor. The settings for the unit are listed in Table 1.

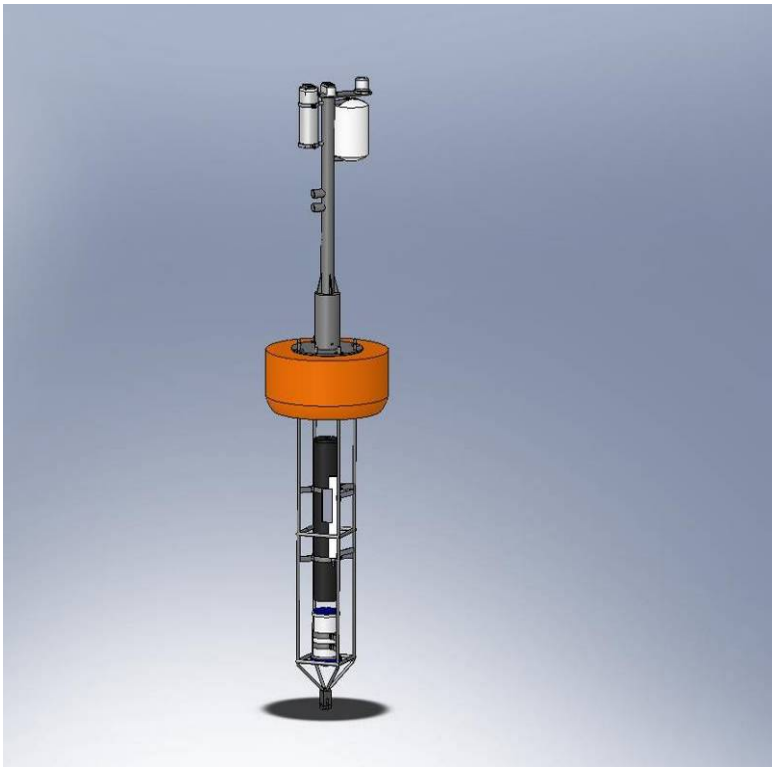

Figure 2. Drawing and a photograph of the Scripps-designed coastal buoy system for measuring stratification and currents at the Point Loma Ocean Outfall.

Figure 3. Photograph of the deployed ocean buoy at the PLOO. The white cylinder on the right is a radar reflector and the cylinder on the left is a GPS tracking device.

Table 1. Settings for the Acoustic Doppler Current Profiler (ADCP) used to monitor subsurface currents at the PLOO.

System Parameter	Setting
Acoustic frequency	300 kHz
Pings per ensemble	25
Ensemble interval	3 minutes
Range cell size	3 meter
Measurement standard deviation	1.4 cm/s
Number of depth cells	33

Measurements of water column stratification were made using temperature sensors located at different depths. For the PLOO buoy, a temperature chain was employed, which consisted of 13 nodes spaced across the water column, each measuring ocean temperature with accuracy of 0.01°C. Measurements at each depth were synchronized to provide a water column profile of stratification at one-hour intervals. Use of the interconnected temperature measurements provided consistent timing across different water depths and eliminated clock drift problems that often occur when individual, self-recording temperature probes are used. The depths of measurement were 2 m, 5.8 m, 7.7 m, 9.6 m, 11.5 m, 15.4 m, 19.2 m, 23.1 m, 30.8 m, 38.6 m, 54.2 m, 69.4 m, and 88.6 m.

Buoy position, currents, and ocean temperature data were transmitted to shore once each hour using an Iridium Satellite modem. Receiving the data in near-real-time allowed observation of present ocean conditions to estimate the rise height and the direction of the PLOO plume. The mooring was deployed just west of the diffuser wye at 32.665N, -117.325W at a depth of 95 m. The all-chain mooring was secured with a 900-lb anchor (Figure 4). The mooring was deployed on April 7, 2010, and subsequently serviced on November 4, 2010. Deployment and servicing were conducted using Scripps research vessels.

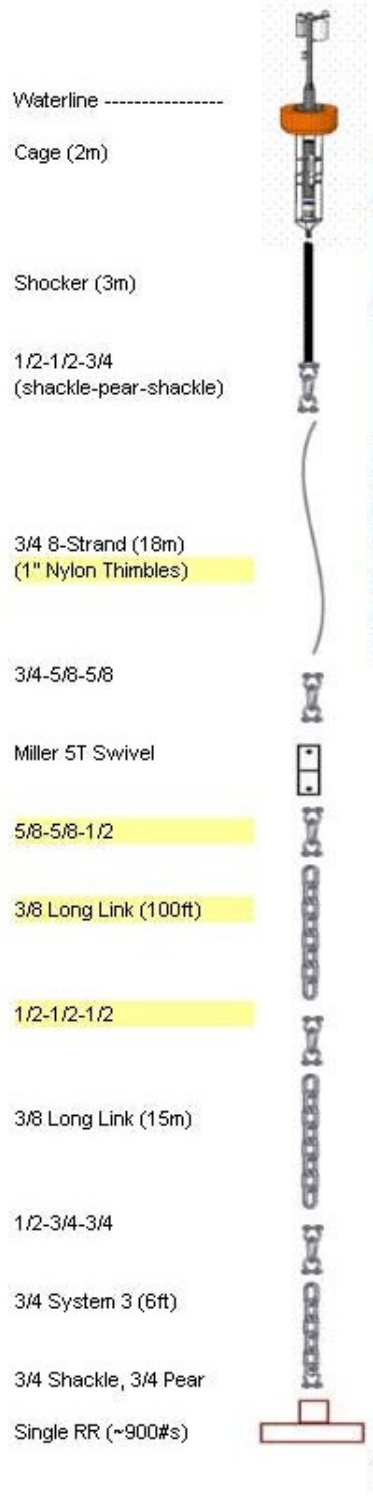

Figure 4. Mooring diagram for the PLOO buoy. The diagram outlines the major mechanical components of the mooring used to keep the buoy in place for the duration of the supplemental monitoring program.

2. Nearshore ADCPs

Two 600 kHz Teledyne Ryan ADCPs (Workhorse Sentinels) were deployed inshore of the PLOO diffuser wye along the 35 m contour (see Fig. 1 – Central and South ADCPs) to supplement the offshore current data generated at the telemetry mooring site. The nearshore ADCPs were deployed on the bottom looking upwards and data were internally stored. The ADCPs were retrieved and redeployed at approximately three-month intervals. Currents were binned at two meter intervals beginning from ~3 m off the bottom to the surface. The ADCPs were also equipped with a temperature sensor. Current and temperature sampling intervals were set to five minutes.

C. Modeling Near-Field Plume

The rise height of a buoyant discharge plume is controlled by the outfall design and density structure with depth in the near-field and ocean circulation in the far-field. The latter is controlled by winds, tides, along-shore pressure gradients, and internal waves. The U.S. EPA Roberts-Snyder-Baumgartner (RSB) plume model (renamed NRFIELD) was applied to the mooring data to predict the height of the plume and its potential to surface in the near-field (Roberts et al. 1989, Roberts 1999a, Roberts 1999b). The NRFIELD model is based on extensive experimental studies on multiport diffusers in density-stratified currents of arbitrary flow described in *Roberts et al*., [1989]. The experiments covered a wide range of parameters typical of ocean outfalls including jet momentum, buoyancy flux, port spacing, stratification, and current speed and direction [*Roberts*, 1999a]. Once these inputs are defined, the model predicts wastefield characteristics at the end of the initial mixing zone (near-field). These include near field dilution, plume rise height, thickness and length of the initial mixing zone. An extensive description of the model basis can be found in *Roberts et al*., [1989] and the model formulation is described in the EPA manual [*Baumgartner et al*., 1994]. The PLOO engineering parameters and the NRFIELD model output are listed in Tables 2a and 2b.

Table 2. A list of the parameters used in the NRFIELD plume model. a) Outfall configuration parameters. b) Model outputs.

(a)

Model inputs	**Input data**
Number of ports	208
Port diameter (m)	0.1
Port spacing (m)	7.32
Discharge depth (m)	93
Diffuser orientation (degrees)	15
Effluent density	0.997
Number of points in density profile	7

(b)

Model outputs
Minimum dilution at the end of the near-field
Rise height (m)
Plume Thickness (m)
Height to level of near-field dilution (m)
Length of the near-field (m)

Ocean density was not directly measured on the mooring. Instead density profiles were estimated using temperature data since the density stratification in Southern California has been found to be strongly dependent on temperature [*Winant and Bratkovich*, 1981, *Bratkovich, 1985*]. Density profiles were thus estimated from measured temperature profiles and climatological estimates of salinity (Millero and Poisson 1981, Fofonoff and Millard Jr. 1983).

D. Autonomous Underwater Vehicle Deployments

Primary mapping of the PLOO plume was performed by an Autonomous Underwater Vehicle (AUV) designed for coastal monitoring. The Remote Environmental Measuring UnitS (REMUS) manufactured by Hydroid LLC (Figure 5) utilizes onboard navigation for vehicle control and can be preprogrammed to map user-driven scenarios based on areas of interest. The vehicle is typically launched by two persons from the boat at a location nearest to the start position and receives a start command from an underwater acoustic control unit called a Ranger. At initial deployment, the vehicle always takes a Global Positioning System (GPS) fix and zeros the pressure sensor to initialize its horizontal and vertical navigation algorithms. After these fixes, the vehicle navigates using underwater transponders with fixed/known locations or by re-acquiring GPS throughout the deployment. Depth is monitored by a pressure sensor and altitude and speed of the vehicle over the seafloor is obtained with an ADCP bottom ping. The Ranger continually queries the vehicle throughout the deployment to gain system status. The vehicle has a 100-meter maximum operating depth and 22-hour battery capacity for surveying at an optimum

speed of 3 knots. This range decreases with increasing speed to eight hours of surveying at five knots. Upon completion of the mission, the vehicle is again recovered by two personnel.

Figure 5. REMUS vehicle on boat prior to mission deployment (GPS, sidescan sonar, ADCP, CTD, backscatter, colored dissolved organic matter [CDOM]).

The AUV includes an array of instrumentation for environmental monitoring. The combination of the CTD and optical sensors (the standard workhorse tools used by boat-based NPDES monitoring programs) placed onto a flexible platform such as REMUS, lends itself well to the problem of plume mapping through surveying changes in ocean properties. The REMUS has four main sections - a nose section, an RD Instruments 1200-kilohertz (kHz) ADCP, a mid-body and tail section. The nose section includes both the Ultra-Short BaseLine (USBL) and Long BaseLine (LBL) acoustic navigation transducers. The sensors used for these studies include a fast response, high resolution, Conductivity, Temperature, and Depth (CTD, Neil Brown Instruments, Falmouth, MA) sensor and an optical fluorometer calibrated to measure backscatter at 650 nm and 880 nm and CDOM with a sensitivity of 0.09 ppb (WET Labs ECO triplet, Philomath, OR). The parameters measured onboard the REMUS vehicle and their usage for discharge plume detection is listed in Table 3.

1. Mission Planning

A challenge in accurately tracking a wastewater plume is the design of an effective sampling plan which adapts to variable oceanographic conditions in the environment [*Ramos et al*., 2002]. For the PLOO, scientists utilized velocity and temperature profile sets to accurately program the REMUS to capture the plume signature. Datasets were reviewed daily to determine whether conditions indicated either northward or southward advection of the plume. The most probable missions would be planned prior to sampling based on near real-time oceanographic conditions at the outfall as monitored by the buoy coupled with plume model predictions.

In the days preceding a monitoring mission, model outputs using telemetered data from the moored buoy instrumentation were analyzed for vehicle path planning. Vertical sampling was constrained by estimates of the plume height and thickness using the U.S. EPA Roberts-Snyder-Baumgartner (RSB) plume model (now renamed NRFIELD) [*Roberts et al*., 1989, 1999a, 1999b]. The AUV was programmed to swim a sawtooth undulation pattern normal to the mean advection of the plume for a depth range based on the predicted rise height and thickness of the plume from NRFIELD outputs (typically between 40 – 90 m). This approach yielded an

approximate profile spacing of 500 m for resolving cross-sections of the plume at varying ranges from the discharge.

Horizontal sampling was constrained with the aid of trajectory estimates made from telemetered buoy ADCP data. Trajectories representing the bulk transport of the water for the entire water column were computed for 72 hours of data and updated on an automated basis with the receipt of the next hour of data (Figure 6). Trajectories were computed from the time series of *u* and *v* velocities from the buoy ADCP. This web-accessible spatial information served as a key decision aid for horizontal path planning of the survey to maximize chances of sampling the plume. When used in conjunction with a 5-hour averaged current profile, REMUS mission paths (dotted line) were developed to spatially optimize plume sampling and minimize measurements outside of the plume. Hourly current velocity profiles were also monitored in the hours leading up to the vehicle deployment to assess if the plume orientation was changing and determine if adjustments were necessary.

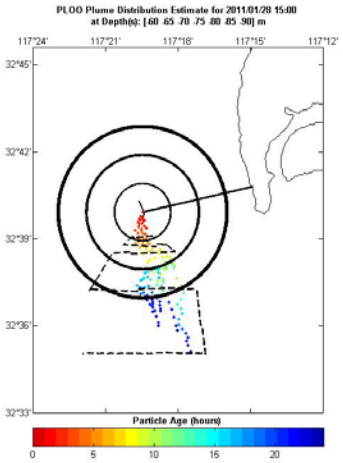

Figure 6. Near real-time PLOO plume trajectory estimated for depths between 60 – 90 m from the PLOO mooring indicating southerly flow. The dotted line denotes the horizontal PLOO REMUS mission programmed to capture plume signature.

Table 3. Onboard sensing capabilities of the REMUS vehicle and application to plume water detection.

Parameter	Ambient Values	Measured Plume Values	Measurement Value
Velocity	N/A	N/A	Subsurface velocity measurements can be used to calculate currents for comparison with fixed mooring assets and to assess changes in currents within the sampling region.
Conductivity (Salinity)	33.7 - 34.2 practical salinity units (psu)	PLOO ≤ .07 - 0.2 psu below ambient	Conductivity measurements are used to calculate salinity values and can measure the freshwater signal of plume water compared to background ocean levels.
Temperature	N/A	N/A	Water temperature measurements are used to estimate ocean stratification, which controls the rise height of a buoyant discharge plume.
Optical backscatter	bb(650) <0.001 bb(880) <0.003	PLOO bb(650) <0.003 bb(880) <0.006	Optical backscatter measured at two wavelengths (650 and 880 nanometers [nm]) is used as an indication of turbidity. The signal measured by this meter is directly correlated to particle concentrations. Higher turbidity measurements are indicative of plume water. The TJR plume is always clear in backscatter due to strong signal, but kelp can easily mask PLOO plume signature in the far field. Kelp forest has values bb(650) <0.01 and bb(880) <0.01. Ratios of the optical backscatter can serve as a proxy for the size distribution of ocean particles.
CDOM (Colored Dissolved Organic Matter)	≤ 4.0 parts per billion (ppb)	≥ 4.2 ppb	CDOM measurements serve as a clear indicator of plume water having values more elevated than ambient seawater.

2. Colored Dissolved Organic Matter (CDOM)

Use of fluorescence for distinguishing plume water from its receiving water has been addressed in earlier literature [Jones et al., 1993; Washburn et al., 1992; Wu et al., 1994]. The authors used chlorophyll fluorescence, a beam transmissometer, a current meter, and a CTD collectively to determine plume location. The work of Petrenko et al. [1997] complimented these findings by utilizing only elevated levels of fluorescence to detect plume waters through the use of a fluorometer with a excitation/emission (Ex/Em) wavelength pair of 228/340 nm. They concluded that such fluorescence (low Ex/Em wavelength) may be useful as a new in situ natural tracer of effluent discharges. The present work builds on this finding by using a compact form factor fluorometer calibrated to measure CDOM, with Ex/Em = 370/460 that is suitable for installation in the nose of an AUV. The sensor was calibrated in a black polyethelene tank (0.3 m diameter x 1.3 m high) through successive dilutions of source effluent from the Point Loma Wastewater Treatment Plant (PLWTP) using clean seawater obtained from the Scripps Pier. Seawater was chosen for the dilute to replicate field conditions. The CDOM fluorometer was suspended in the middle of the tank to eliminate any biases from optical reflections and the tank

was kept dark to prevent ambient light from influencing the sensor reading. Successive dilutions from 1:1 to 1:600 (by volume) were conducted, and the sensor was configured to sample at 1 Hz for several minutes between dilution levels. The source had a measured CDOM concentration of 121 ppb and the ambient seawater CDOM concentration was 3.96 ppb which was accounted for in the calibration. The CDOM calibration curve showed that the sensor has a well-behaved response to the range of dilutions used described by D = F(CDOM (ppb))

$$D = 2*10^{-5}*(CDOM)^2+6*10^{-3}*(CDOM) - 8*10^{-4} \qquad \text{(Eq. 1)}$$

with $R^2 = 0.99$, (plotted on log plot to show full range of dilution; Figure 7), with the detectability of the highest dilution ratio limited by the background seawater levels. For a dilution range of 50 - 600 (levels expected to be sensed in the field), the CDOM levels concentrations ranged from 0 – 2.5 ppb after the background CDOM concentration is accounted for. We note that effluent CDOM levels will vary from plant to plant due to varying levels of treatment, making this calibration specific to the PLWTP. The sensor calibration (eq. 1) was applied to the AUV-based CDOM measurements in order to infer plume dilution in the following sections.

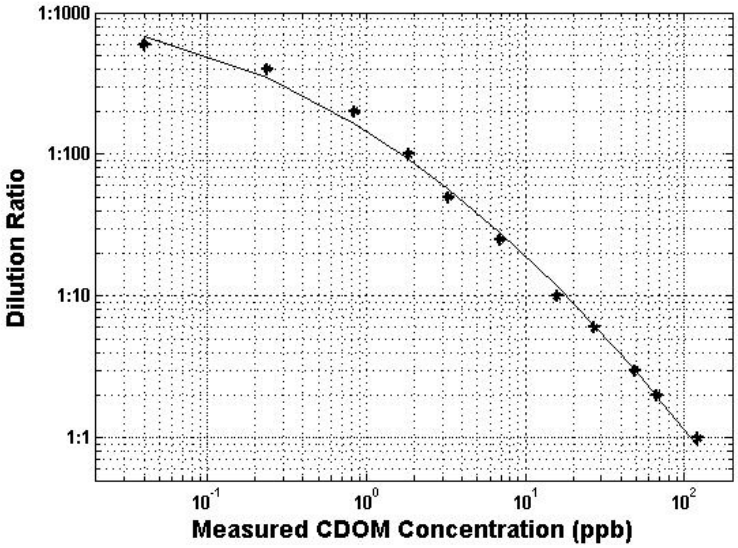

Figure 7. CDOM calibration curve for successive dilutions of source effluent from the Point Loma Wastewater Treatment Plant.

A principal challenge in tracking an outfall plume is the spatial and temporal variability of ocean currents and stratification in coastal waters which, without the aid of recent measurements, limits plume sampling far from the outfall due to uncertainty in the plume's location. Often the plume is missed by traditional *a priori* grid-shaped sampling designs due to the plume's spatial patchiness and the limited range of the freshwater signature of the plume. For example, *Terrill* [2009] shows that monthly sampling of a discharge offshore San Diego using traditional conductivity, temperature, and depth (CTD) sampling on pre-defined grids were able to detect the discharge plume only twice out of 16 monthly surveys. The work performed

on the South Bay Ocean Outfall (SBOO) determined that the plume had an elevated CDOM signature that proved to be a better natural tracer than traditional monitoring methods. CDOM exists naturally in seawater and freshwater environments and generally consists of decaying organic matter from living organisms. Nearshore CDOM has both marine and terrestrial sources due to riverine input. CDOM concentrations near shore may be further elevated by human activities such as logging, agriculture, and wastewater discharge. Based on this work, elevated CDOM levels from discharged wastewater were used as the primary plume tracker for PLOO monitoring missions.

III. RESULTS AND FINDINGS

A. Shelf Hydrographic Observations

1. Telemetry Mooring

A summary of the vertical structure of ocean temperature and water velocity is provided in this section. Figure 8 (top) presents a color contour plot of time records of ocean temperature at the outfall site. The contour is created by data from the 13 temperature probes that span the water column. The seasonality of the ocean temperatures is clearly evident in the upper water column (<30 m), with warmer waters and a stratified ocean present during the dry season (April through September) and remaining through the beginning of the wet season (October). Cooler waters and weak stratification characterize the ocean conditions in the upper water column during the remainder of the wet season (November through March). Below 30 m, the water column remains weakly stratified throughout the year. The only significant fluctuations in temperature occur at the end of December. Figure 8 (bottom) illustrates the temporal variability of the temperature time series from December 13-30, 2010 during an observed down-welling event. On December 22, 2010, the warmer surface water is advected down the length of the water column creating a well-mixed layer of warm water to a depth of approximately 80 m.

Alongshore winds are a common forcing mechanism of coastal upwelling and downwelling. When wind flows parallel to a long coastline for an extended period, a steady state develops and net transport of the surface waters will be 90^{o} to the right of the wind direction [*Ekman*, 1905]. Therefore, periods of wind-induced downwelling are associated with persistent southerly and onshore winds. However, the warming event observed on December 22, 2010, does not appear to be a result of wind induced downwelling as velocity profiles show a consistent northwest current in the hours preceding the downwelling event (Figure 9). If Ekman transport was causing the downwelling, an on-shore current would be evident in the study area. Also, no significant on-shore winds were measured during this time frame, eliminating the wind as a possible mechanism. From Figure 9, the maximum downward velocity (~ 0.5 m/s) occurs for only a 1-hour interval with lower velocities (~0.1 m/s) observed in the hour before and after. Similar maximum vertical velocities in the upward direction are seen 9 hours earlier, also for only a 1-hour interval. This pattern of high upward velocity followed by high downward velocity suggests the presence of an internal wave propagating through the study area. Internal waves will be discussed in more depth in a later section.

A way of assessing the general trends of the currents at the site is to examine the depth-averaged flow. For this analysis, the currents are vertically averaged and a 25-hour time averaging window is used to average out the tidal motion to make the subtidal motions more visible. The subtidal motions are most relevant for tracking plume behavior since tidal motions do not result in net transport. Figure 10 presents the depth and tidally filtered velocity records for the site. The figure shows the temporal variability of the currents from April 2010 to April 2011. However, graphically presenting the dense data over a 12-month period does not give one an indication of the shorter time-scale fluctuations in the ocean current. As an example of the variability of the regions currents, a time series of velocities for the time period from December 21-28, 2010, is provided in Figure 11. The figure illustrates the changes in the currents that can occur over a few days, with the flow dominant northward at the start of the record and changing to a southward flow in the period of 3 days.

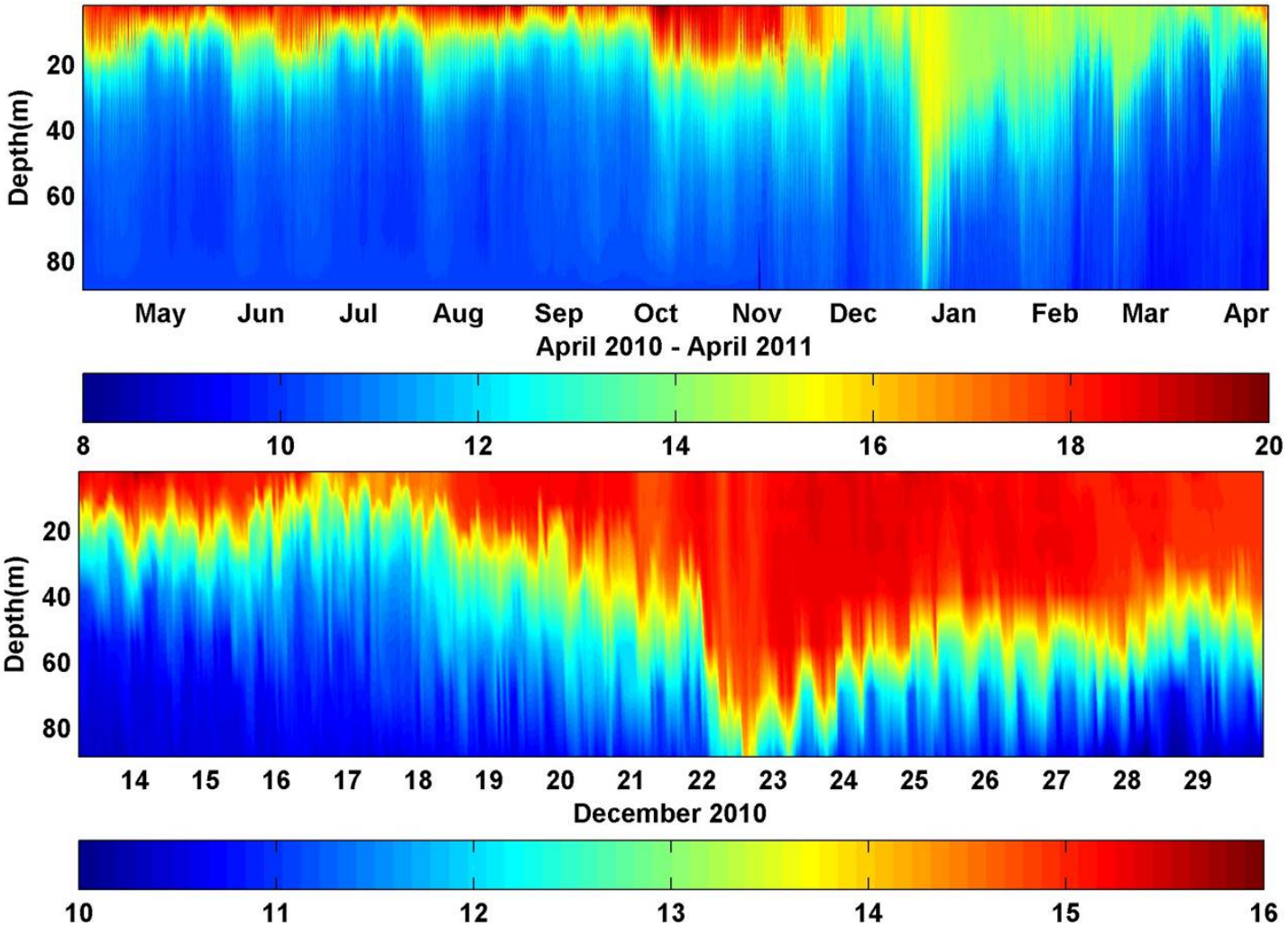

Figure 8. Time series of ocean temperature. Top:Temperature time series during entire mooring sampling period. Bottom: Temperature time series from December 13-30, 2010 illustrating an observed down-welling event. The color bars indicate the temperature in Celsius.

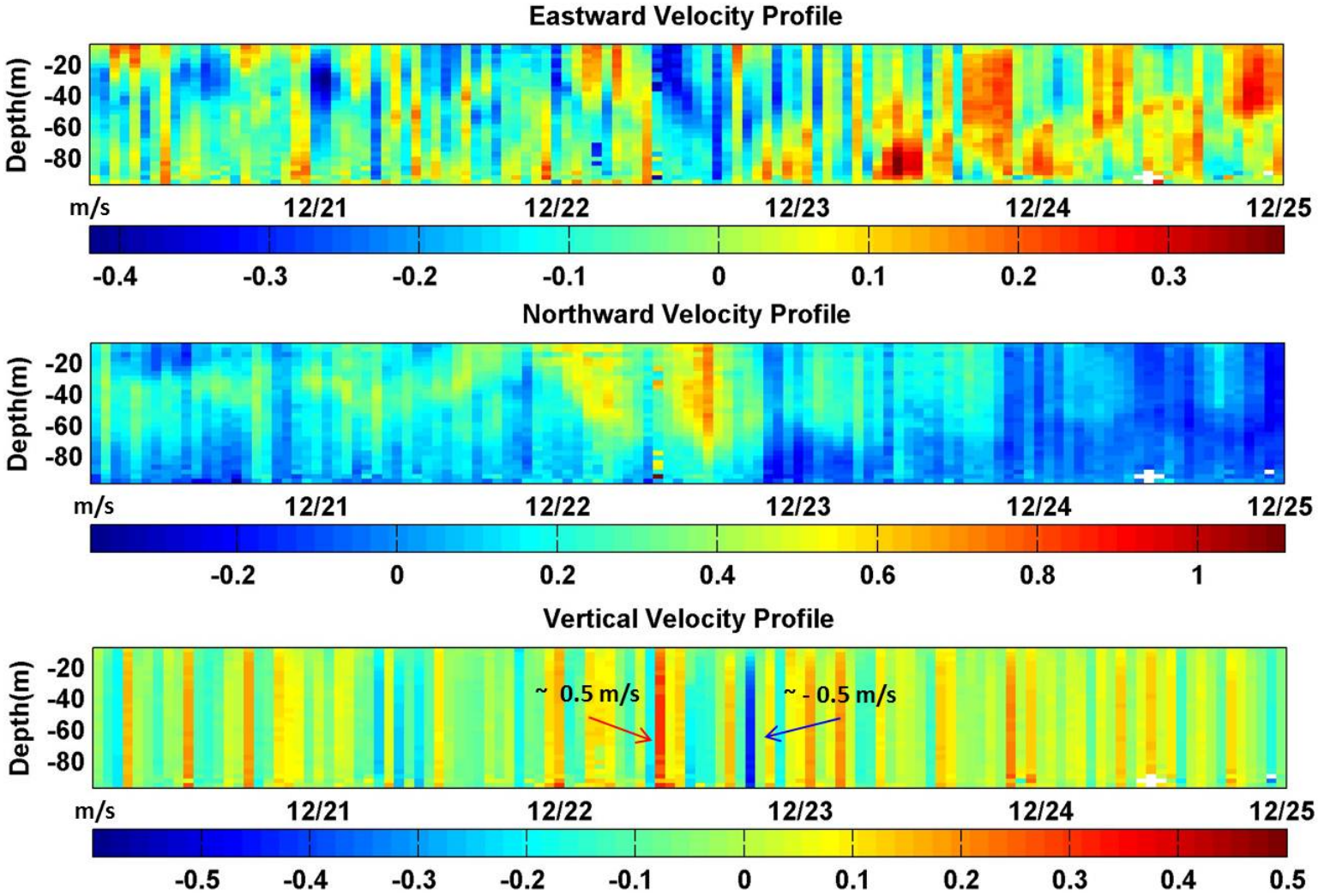

Figure 9. Eastward, Northward, and Vertical Velocity profiles from December 20-25. A significant and consistent northwest current is seen in the hours preceding a downwelling event on December 22, at approximately 18:00.

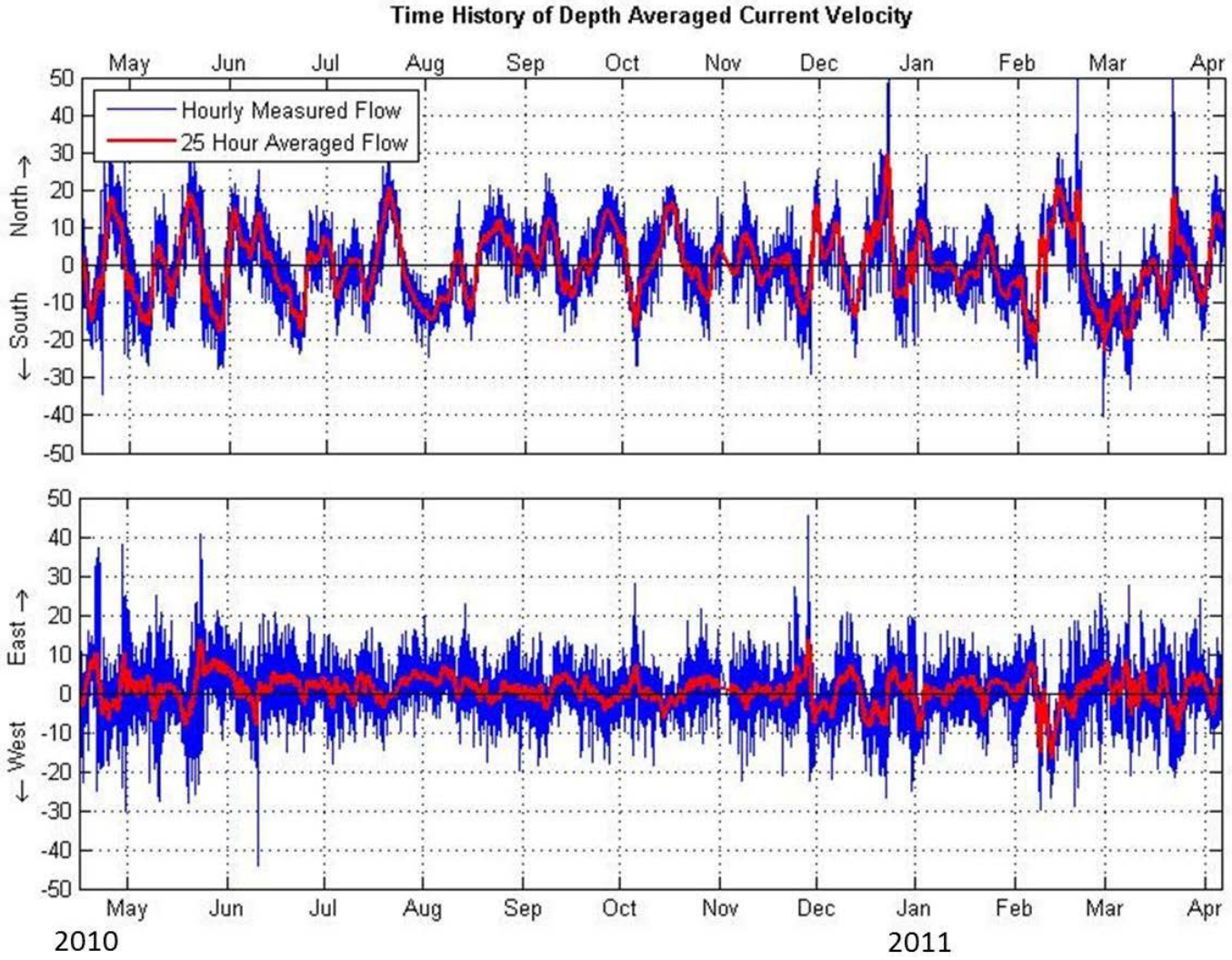

Figure 10. Depth averaged currents for the north/south and east/west components at the PLOO mooring site. The blue line is hourly data while the red line is a 25-hour running average to remove the tides.

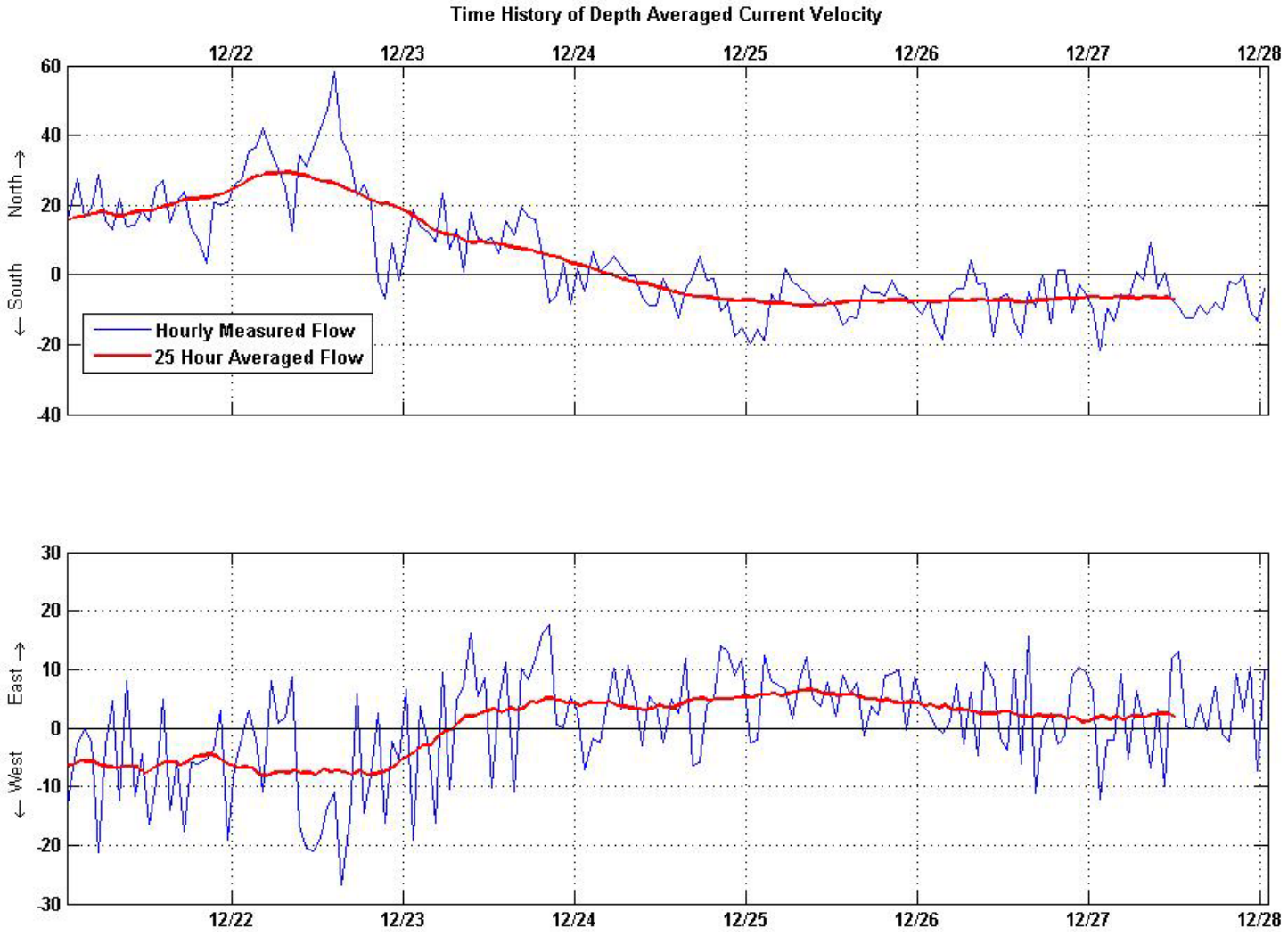

Figure 11. Depth averaged currents for the north/south and east/west components at the PLOO mooring site. The blue line is hourly data while the red line is a 25-hour running average to remove the tides.

2. Hydrography of the Inner Shelf

Currents over the inner shelf along the 35m contour (see ADCP locations in Figure 1), were similar to the currents observed over the outfall diffusers. The largest source of variability in the subtidal frequency band included alternating periods of approximately unidirectional alongshore flows (oriented northwest to southeast) throughout the water column persisting for periods of a few days to a little more than a week (Figures 12 and 13). Temperature increases at subtidal frequencies near the bottom typically coincided with northerly flows. Vertically sheared flows were typically observed during transitions between the low frequency northward and southward flows (Figure 14). There did not appear to be a seasonal pattern in the duration and frequency of the lower frequency oscillating flows. Near bottom tidal frequency currents were oriented mostly cross-shore, driven by the internal tide (Figure 15) with onshore currents observed just prior to, and during, temperature decreases indicating upwelling. The strong downwelling event observed at the mooring ADCP in December of 2010 was also observed at both the central and southern Pt. Loma 35 meter sites (Figure 15).

Currents among the two inner shelf study sites, while significantly correlated at most depths, exhibited notable differences. The largest difference was the magnitude of cross-shore flows in both the tidal and subtidal bands (Figure 15). Cross-shore currents in the middle and lower water column at the south site were typically two to three times as great as the central site (Table 4, Figure 16). Vertical velocities at the two sites indicate that the central site is an area of divergence with upward velocities near surface and downward velocities near bottom while the opposite is true for south Pt. Loma where vertical velocities appear convergent. Clearly, upward movement in the bottom of the water column at South Pt. Loma is greater than that for central Pt. Loma indicating that if the outfall plume broached the 35m contour and approached shore, the southern portion of the Pt. Loma nearshore shelf would be most impacted. This is further supported by the greater magnitude cross-shore velocities observed at South Pt. Loma. However, plume contact with this portion of the inner shelf is unlikely given observed and modeled plume trapping depths.

Horizontal and vertical velocities near the bottom at South Pt. Loma (tidal band) were analyzed using EOF analysis since it appears that the south Pt. Loma shelf is the most likely area to be impacted by the plume if it transgressed close to shore (see Table 5 for EOF loadings). The first mode accounted for ~55% of the overall variability among vertical and horizontal velocity constituents. Mode 1 was characterized as a combination of southeastward currents coincident with upward vertical velocities and conversely, northwestward currents coinciding with downward vertical velocities. Subtidal band currents exhibited similar behavior. Southeastward and upward vertical velocities predominated (Figure 17) during the study period of 2010-2012. The first had a strong effect on temperature, with temperature decreases slightly preceding and coinciding with increases in Mode 1 (Figure 18), further indicating that upwelling was accompanied by southeastward currents. Mode 1 was significantly negatively correlated with temperature changes ($r = -0.41$, $p<0.001$).

Table 4. Means of current components at the inshore South and Central Pt. Loma ADCP 35m contour study sites. Means of signed components (indicating direction) and means of absolute values (in parenthesis) are listed (u – cross-shore, v – alongshore, w – vertical

	Central			South		
	u	**v**	**w**	**u**	**v**	**w**
Near surface	237.2 (308.1)	-76.5 (291.9)	9.9 (19.0)	217.6 (417)	-133.8 (365)	-11.7 (24.7)
Midwater	1.2 (25.2)	10.2 (47.5)	0.1 (4.7)	3.06 (76.8)	3.6 (71.8)	1.3 (6.3)
Near bottom	-4.1 (28.9)	4.9 (33.1)	-0.8 (3.1)	-9.3 (54.2)	2.9 (45.3)	0.2 (4.3)

Table 5. Loadings and eigenvalues resulting from EOF analysis of near bottom velocities (u,v,w) at the South Pt. Loma station.

	Component	**Mode 1**	**Mode 2**
EOFs	**u**	0.65	~0
	v	-0.53	0.71
	w	0.54	0.70
	Eigenvalue	1.68	0.85

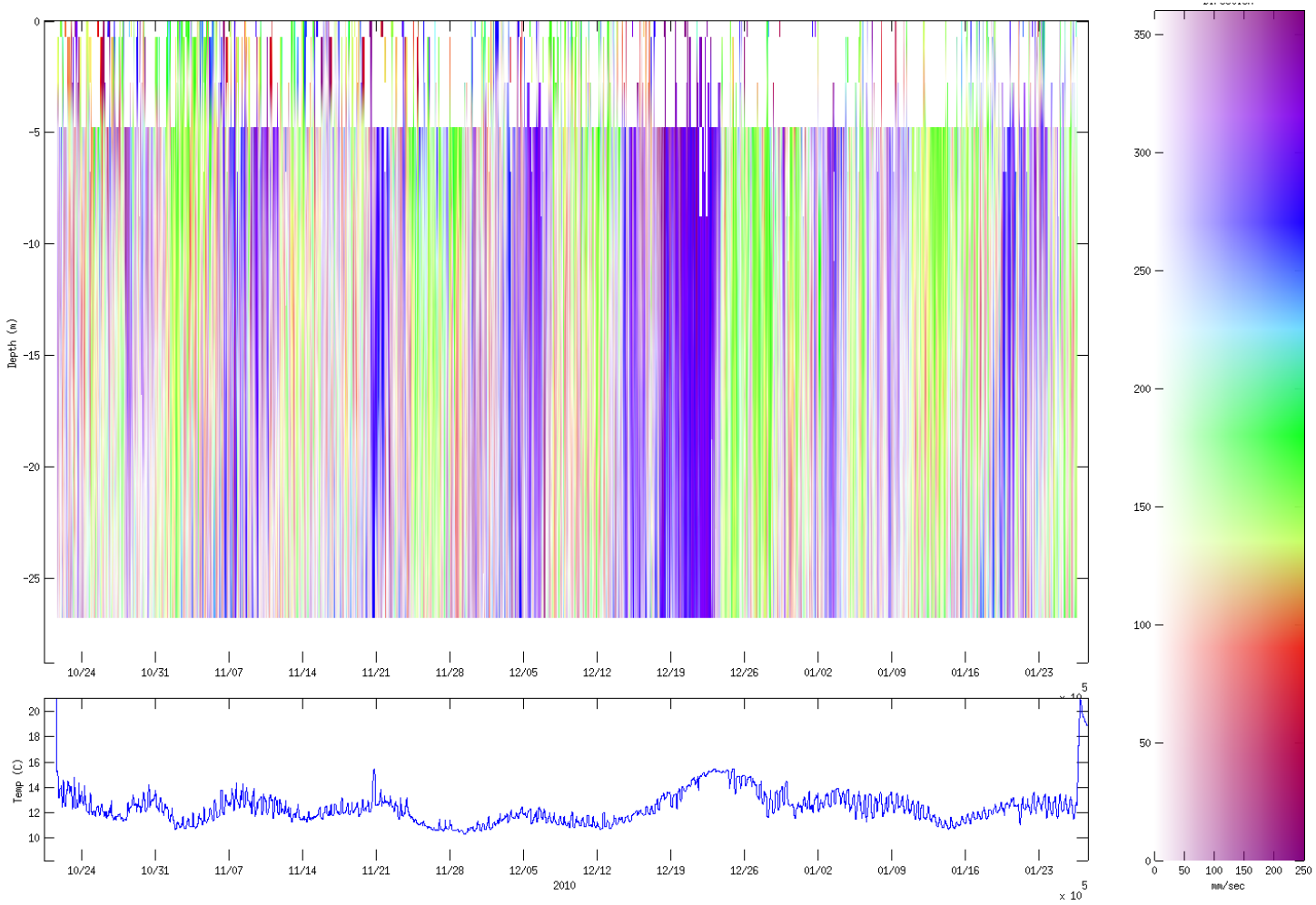

Figure 12. Currents (top panel) throughout the water column and bottom temperature (bottom panel) at the South Pt. Loma ADCP study site – depth 33m from October 22, 2010 – January 25, 2011. Colors indicate current direction, and intensity indicates magnitude (see legend).

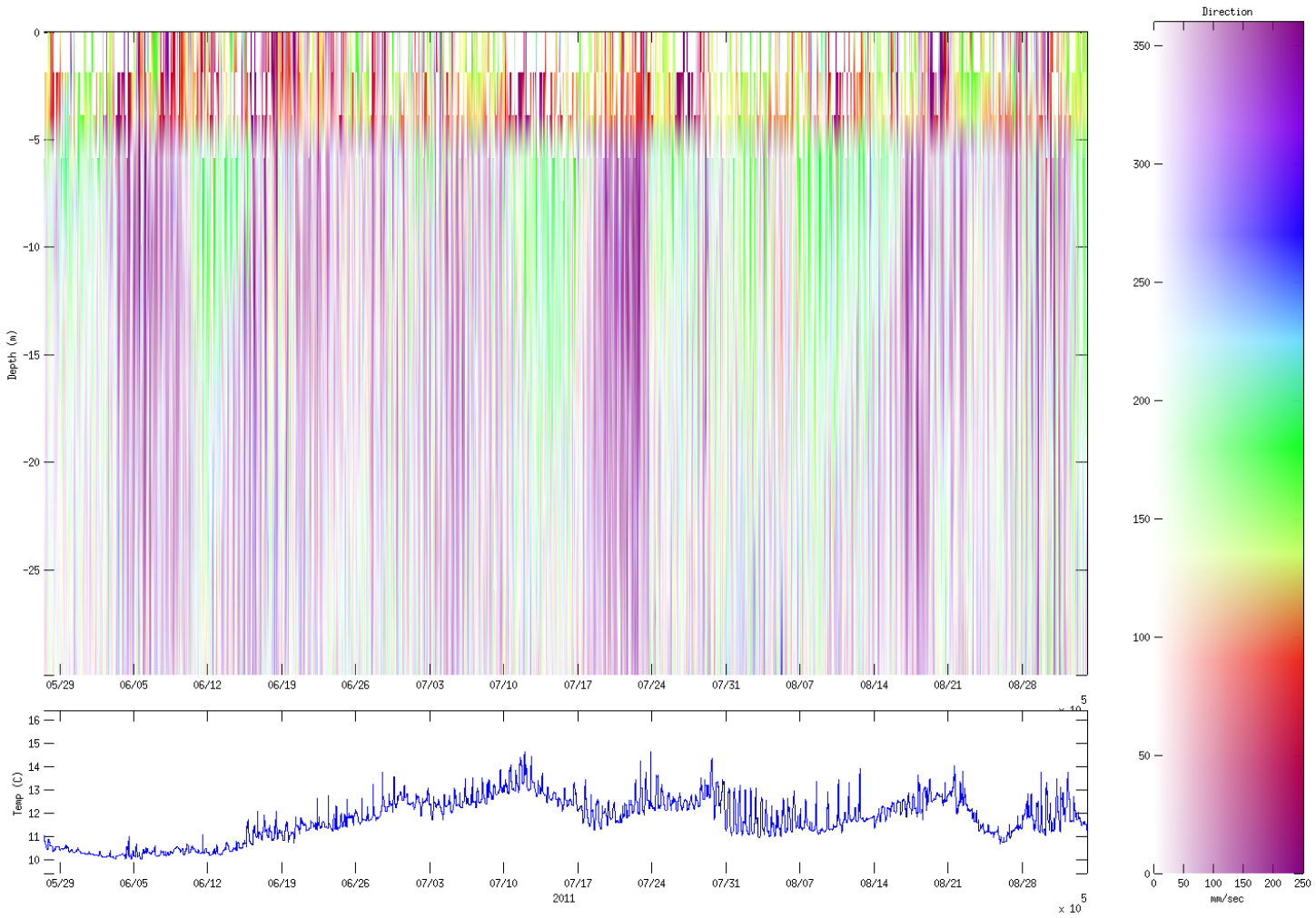

Figure 13. Currents (top panel) throughout the water column and bottom temperature (bottom panel) at the South Pt. Loma ADCP study site – depth 33m from May 28, 2011 – September 1, 2011. Colors indicate current direction, and intensity indicates magnitude.

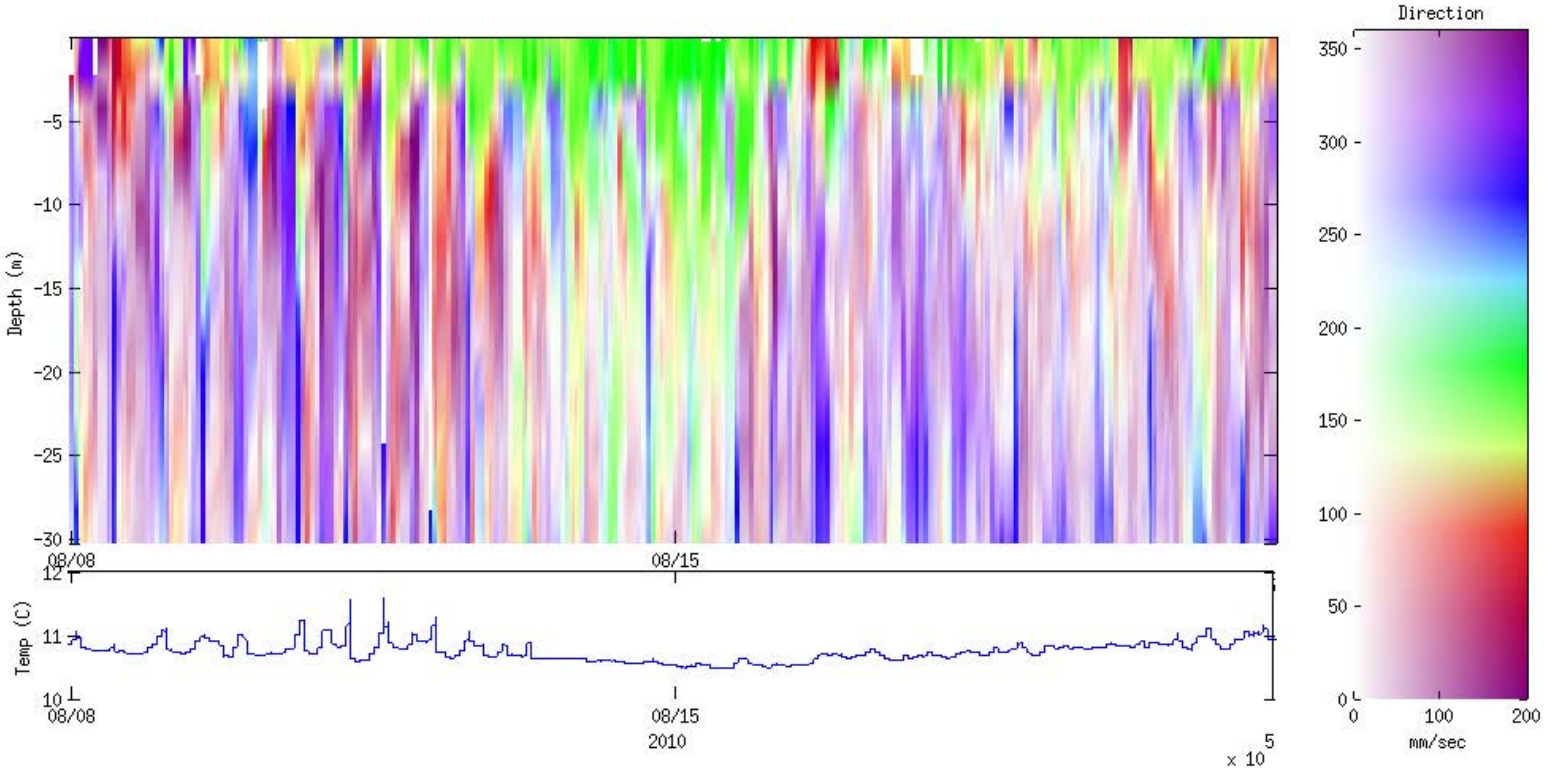

Figure 14. Currents (top panel) throughout the water column and bottom temperature (bottom panel) at the South Pt. Loma ADCP study site for a 2-week period – water depth 33m, from August 8, 2011 – August 22, 2011.

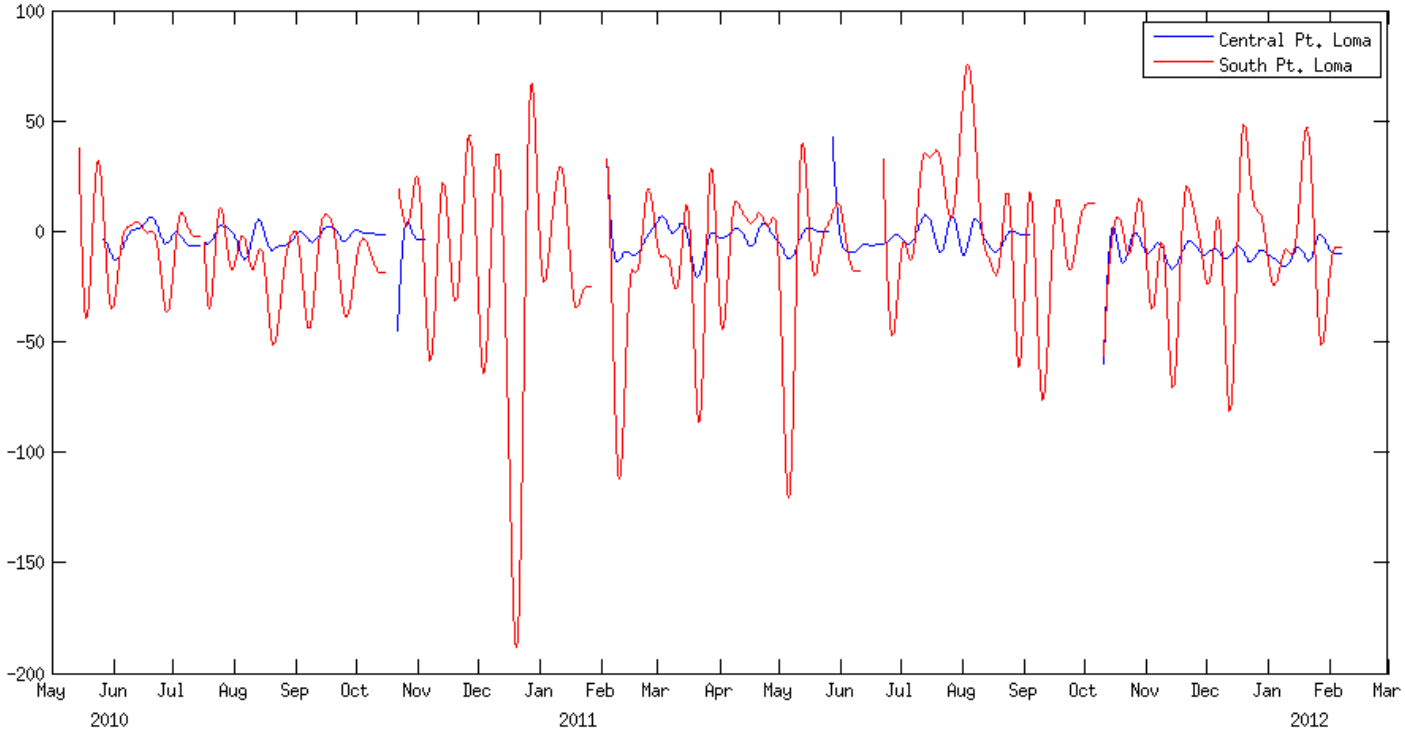

Figure 15. Near bottom cross-shore (E-W) currents (mm $s^{-1)}$ at the Central (blue) and South (red) ADCP study sites for the entire study period. Cross-shore currents at the both the subtidal (pictured) and tidal frequencies were much greater at south Pt. Loma.

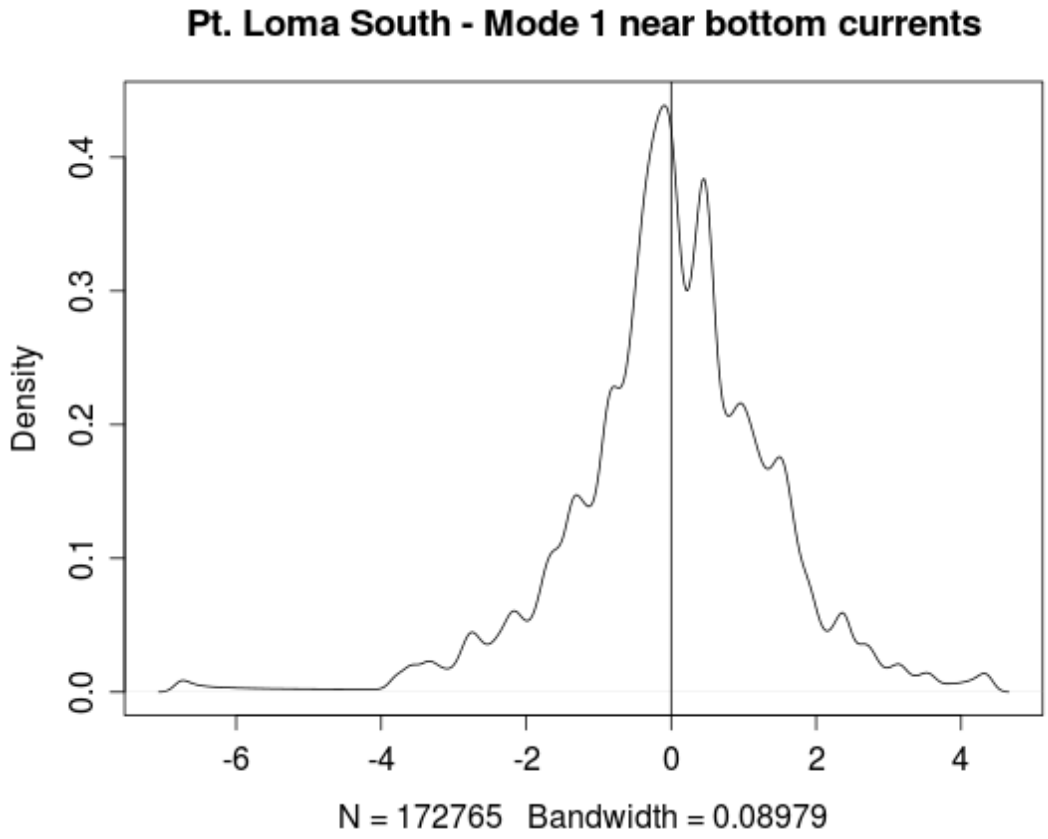

Figure 16. Probability density of Mode 1 currents indicating that Mode 1 was most frequently positive indicating southeastward and upward currents near the bottom at the South Pt. Loma ADCP study site. Moderate positive values were most frequent for Mode 1.

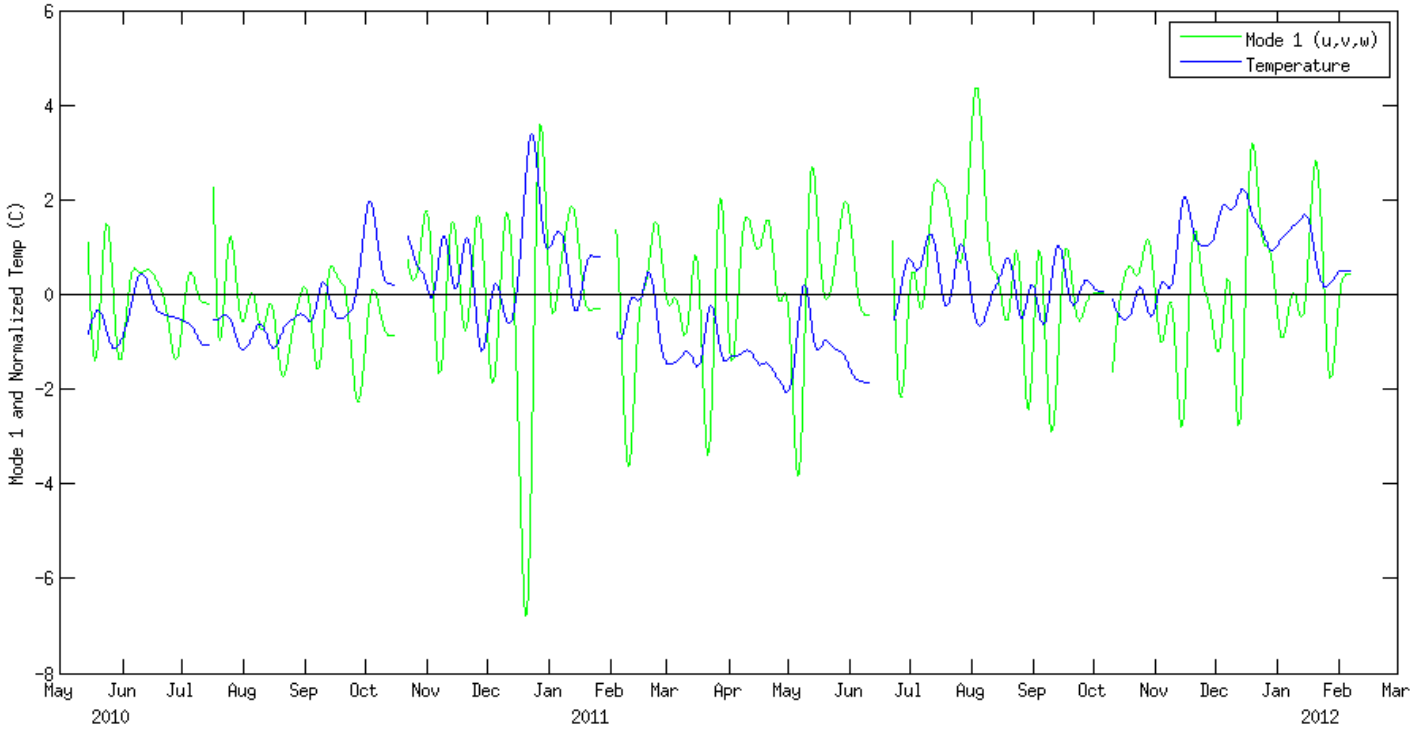

Figure 17. Time series of first mode of EOF of currents at South Pt. Loma near the bottom (green). Velocities were first filtered using a 5-day lowpass filter to eliminate higher frequency variability. The first mode captured >55% of the variability of cross- shore, alongshore, and vertical velocities. Bottom temperature (also lowpass filtered) is shown in blue.

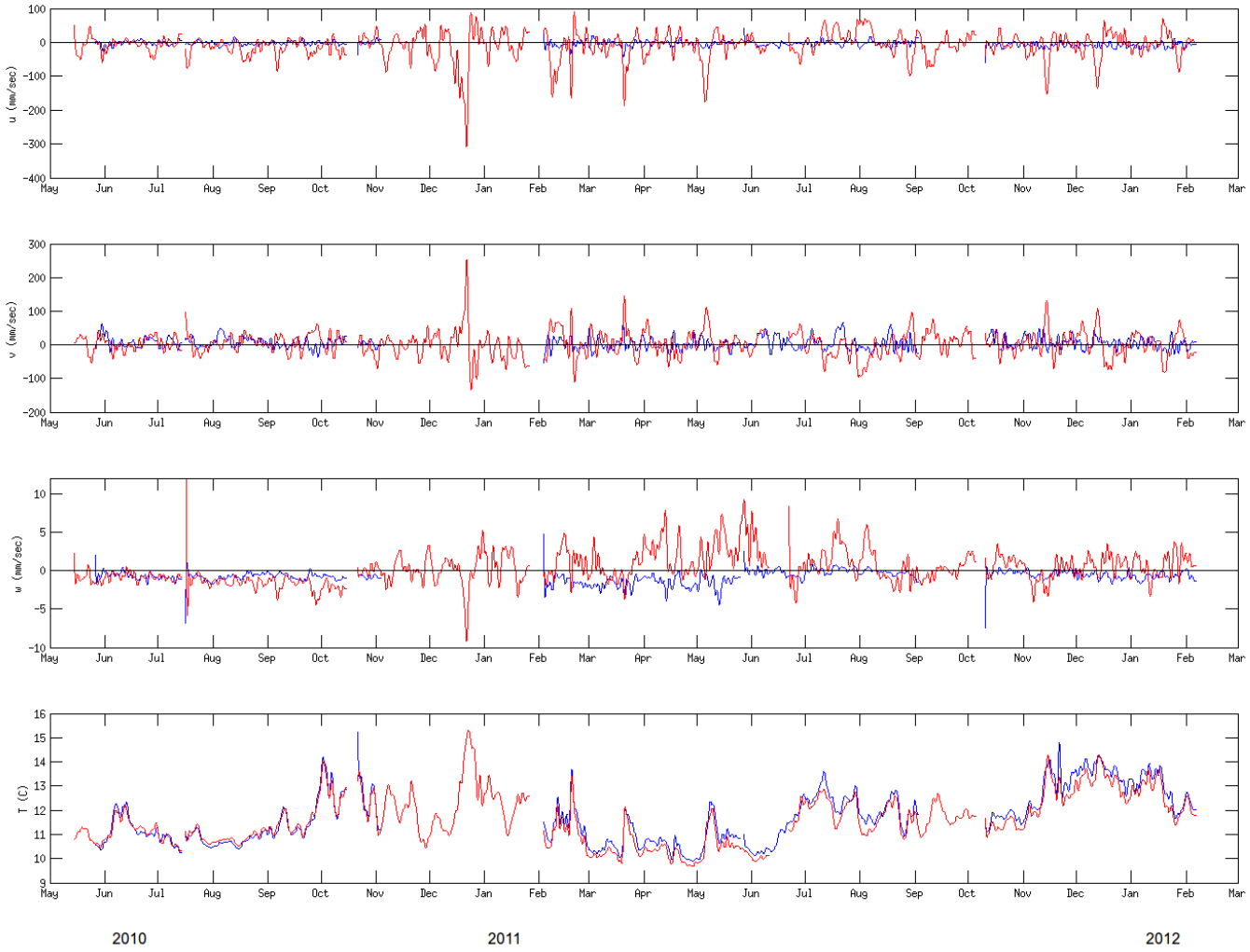

Figure 18. Times series of near bottom currents and temperature (u,v,w, and T) observed at the central (blue) and southern (red) Pt. Loma 35m ADCP stations. Data were lowpass filtered to remove tidal frequencies.

B. Modeling Plume Rise Height

The predicted rise height and bottom depth of the plume, computed hourly for the 12-month record, are shown superimposed with the ambient ocean density for the period of the program (Fig. 19). The plume height is highly dependent on the stratification. The model predicts the plume to rise through the weakly stratified bottom layer until it intersects with the strongly stratified upper layer. A range of rise heights between the depths of 20-30 m was typical during the months of April 2010 to October 2010, while warm waters extended to a depth of 30 m from October 2010 through November 2010 causing stronger stratification at these depths which suppresses the predicted rise height to a depth of approximately 40 m. During the downwelling event on December 22, 2010, the higher density water advected from the surface was predicted to limit rise height to a depth of 60 m.

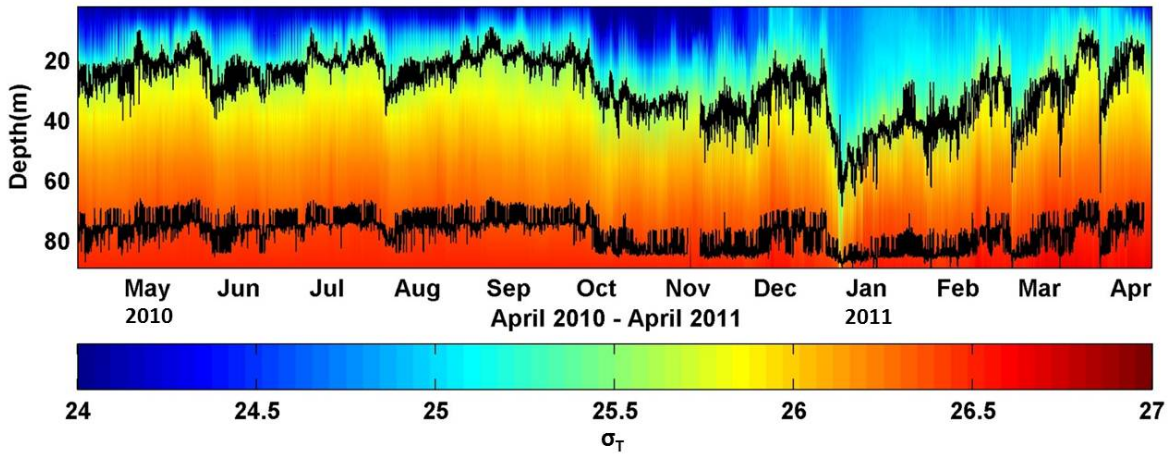

Figure 19. Density structure at the PLOO from April 2010 to April 2011. Also shown are the rise height and plume base estimated using the NRFIELD buoyant plume model. The estimated time-dependent depth extents of the plume are bound by these two black lines. No surfacing events were evident.

C. AUV Plume Surveys

A total of 21 AUV plume sampling missions were conducted between April 2010 and April 2011. Plume sampling dates and general ocean conditions are summarized in Table 6. Monitoring missions were performed on low wind/wave days to assist in deployment and recovery of the REMUS.

REMUS monitoring missions of the PLOO plume were performed when both high and low stratification conditions were present. Generally, the plume was advected either North or South for all missions, with exceptions for the February 28, 2011 and March 3, 2011 (minimal current), April 22, 2011 (variable - changing direction in the hours preceding a mission) and the June 16, 2010 and December 8, 2010 monitoring missions in which an onshore flow was observed (Table 6). The maximum observed plume range is directly dependent on REMUS path planning. Missions conducted on October 14, 2010 and October 28, 2010 included widely spaced transects that allowed for a final transect at approximately 10 km from the outfall diffusers. These missions were designed to capture the extent of the plume and its mixing far

from its source. Conversely, missions from February 25, 2011 through April 22, 2011 focus on the plume mixing nearer to the outfall.

Table 6. Summary of ocean conditions and observed plume ranges for days that REMUS surveys were conducted.

Date	Stratification			Dominant Along-shore Current	Dominant Cross-shore Current	Current Magnitude (m/s) *	Max Observed Plume Range ᵗ(km)
	Subjective	ΔT (°C)	mld (m)				
2010/04/15	Weak	4	5	**North**	**Minimal**	**0.07**	3.3
2010/05/19	Strong	6	3	**North**	**Off-shore**	**0.12**	3.3
2010/06/16	Strong	8.5	2	**Minimal**	**On-shore**	**0.1**	2.2
2010/06/25	Strong	7.5	1	**North**	**On-shore**	**0.1**	2.1
2010/07/14	Weak	4	5	**South**	**On-shore**	**0.1**	4
2010/08/03	Strong	6	4	**South**	**Off-shore**	**0.07**	5.1
2010/09/01	Strong	6	6	**North**	**Minimal**	**0.1**	7.3
2010/10/14	Strong	9	8	**North**	**Off-shore**	**0.17**	9.7
2010/10/28	Strong	8	11	**South**	**On-shore**	**0.11**	9.2
2010/11/16	Strong	6	11	**South**	**Off-shore**	**0.05**	2.9
2010/11/30	Weak	4	5	**North**	**Off-shore**	**0.15**	9.5
2010/12/08	Weak	4	10	**Minimal**	**On-shore**	**0.09**	1.9
2010/12/16	Weak	4	5	**North**	**Off-shore**	**0.05**	2.8
2011/01/21	Weak	4	12	**North**	**On-shore**	**0.13**	1.2
2011/01/28	Weak	4	11	**South**	**Minimal**	**0.18**	9
2011/02/08	Weak	5	3	**North**	**Off-shore**	**0.11**	8.4
2011/02/25	Weak	5	8	**South**	**On-shore**	**0.16**	1.7
2011/02/28	Weak	4	13	**Minimal**	**Minimal**	**0.03**	2.2
2011/03/03	Weak	4.5	7	**Minimal**	**Minimal**	**0.03**	1
2011/04/15	Strong	6	11	**South**	**Minimal**	**0.15**	0.3
2011/04/22	Strong	7	4	**Variable**	**Variable**	**0.07**	1.4

ᵗ Range taken from Intermediate Diffuser Wye

* Average current magnitude between depths of 60 - 90m

The maximum REMUS operating depth for missions between April 15, 2010 and December 8, 2010 was 70 m. (Recall that the PLOO outfall discharges at an approximate depth of 93 m.) Rise height model predictions generally ranged between 20 – 40 m from April 2010 through November 2010 which led to consistent detections of the plume above 70 m. The depth range was extended to 80 m for missions from December 8, 2010 to February 8, 2011 and finally to a maximum depth of 90 m for the remainder of the missions. The range increase was in response to lower observed plume rise heights due to the change in stratification conditions from December 2010 to January 2011 (Table 6).

1. Summary of AUV Plume Survey Findings

Visualizations of the PLOO plume provide some examples of plume detection and spatial distribution. The August 3, 2010 mission successfully tracked the plume over 5 km downstream of its source in a low-current regime (Figure 20). The maximum mission depth was chosen at 70 m to maximize spatial coverage of the plume in the far-field. Backscatter at 650 nm also distinguishes the plume from the surrounding waters, however as distance increases from the outfall, the signature significantly diminishes, making plume tracking difficult (Figure 21). The February 25, 2011 mission was designed to track the plume nearer to its source (< 1 km) in a high current regime and was sampled to 90 m depth (Figure 22). The datasets encapsulate a wide range of oceanographic conditions, making them ideal illustrators of the AUV's plume monitoring capabilities using the natural tracer CDOM.

Temperature and salinity (T-S) diagrams colored by CDOM-based dilution values for each survey mission are shown in Figure 23. The salinity data was "de-spiked" using the recursive filter discussed by *Schmitt et al*. [2005]. Evaluation of the data using this method allows the

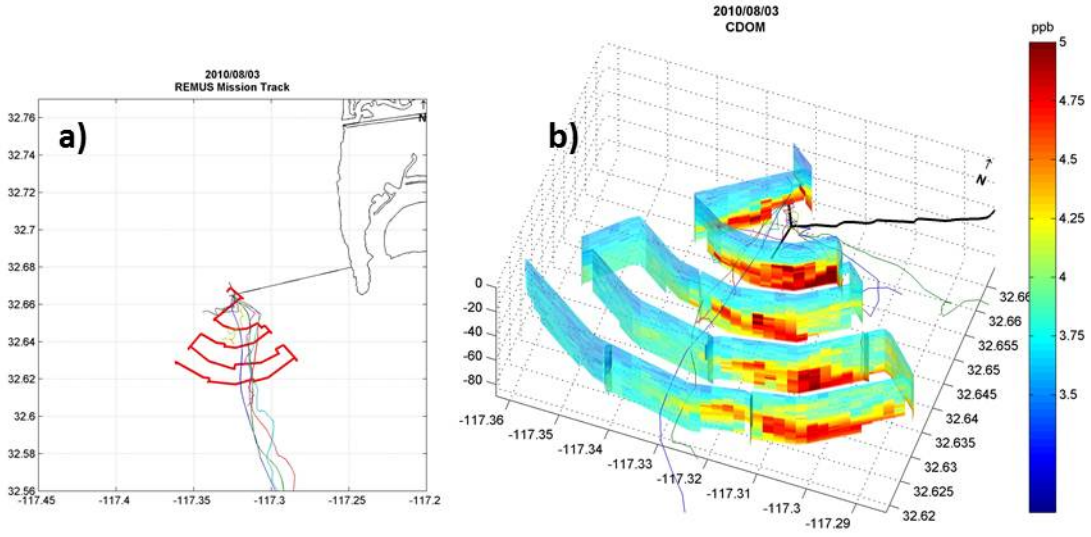

Figure 20. a) REMUS vehicle mission track (red) extending approximately 5 km south of PLOO (shown in black) for sampling conducted on August 3, 2010. Colored lines indicate the estimated plume trajectory based on PLOO buoy velocity profiles. b) Elevated values of CDOM (>4 ppb) indicate high concentrations of organic matter in the PLOO plume. The PLOO is shown in black with the observed plume toward the south-southeast. The plume trajectory (colored lines) is estimated from the PLOO buoy velocity profiles.

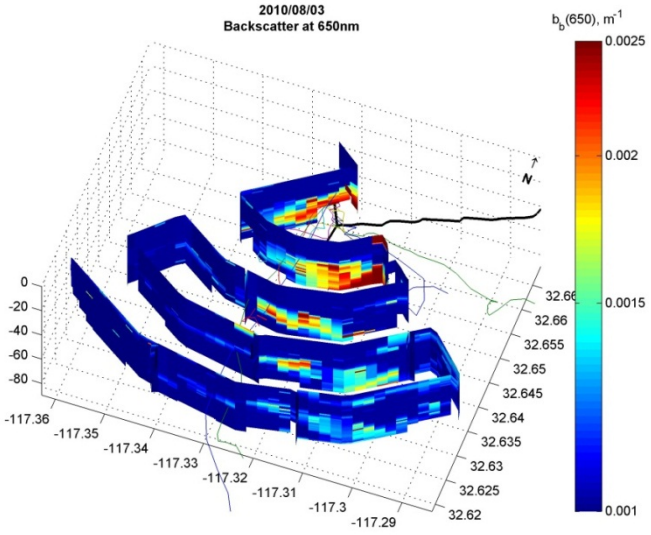

Figure 21. Elevated values (>0.0013m-1) of optical backscatter at 650 nm indicate elevated turbidity in the PLOO plume. The PLOO is shown in black with the observed plume toward the south-southeast. The plume trajectory (colored lines), estimated from the PLOO buoy velocity profiles, suggest the plume advects east until a depth of 60 m where the currents change to a southerly flow.

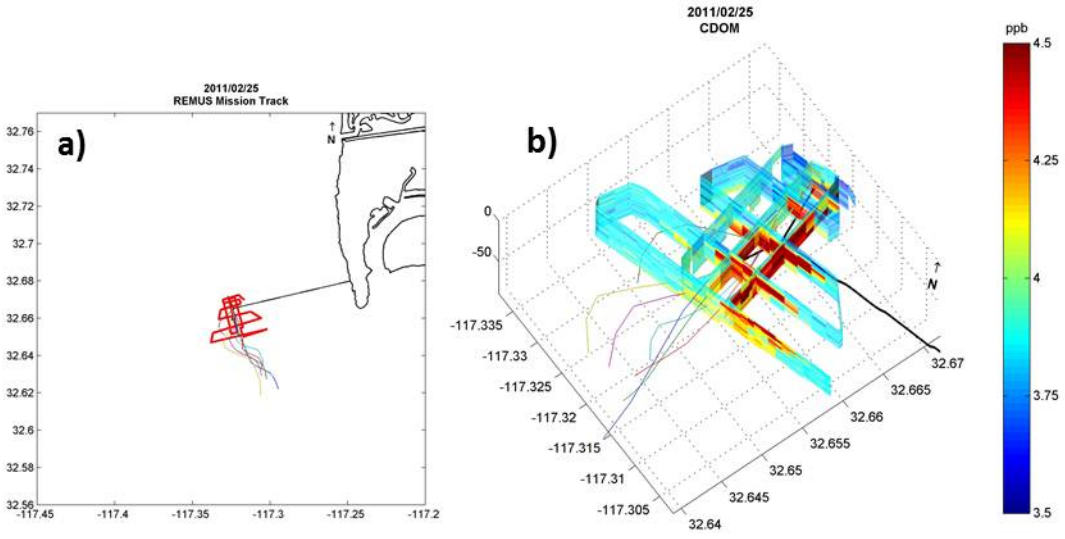

Figure 22. a) REMUS vehicle mission track (red) extending approximately 1 km south of PLOO (shown in black) for sampling conducted on February 25, 2011. Colored lines indicate the estimated plume trajectory based on PLOO buoy velocity profiles. b) Elevated values of CDOM (>4 ppb) indicate high concentrations of organic matter in the PLOO plume. The PLOO is shown in black with the observed plume toward the south. The plume trajectory (colored lines) is estimated from the PLOO buoy velocity profiles.

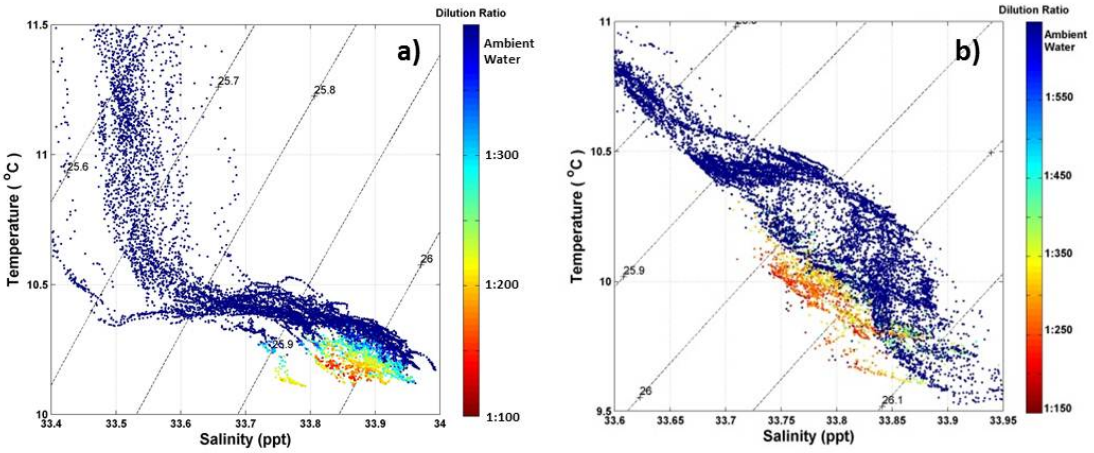

Figure 23. T-S diagram as a function of computed dilution ratios for the August 3, 2010 (a) and February 25, 2011 (b) PLOO missions. The dilution ratio (via CDOM measurements) clearly shows the plume's water mass properties as relatively fresh compared to ambient waters. The diagonal lines in each figure represent lines of constant density.

water mass associated with the plume to be easily identified as a distinct water mass, with the lowest dilution values (i.e. high CDOM) typically having low salinity. Previous work used these salinity signatures and initial mixing lines to estimate dilution near the diffuser [*Washburn et al*., 1992]. The plume water in the survey area typically mixed to the point of having little to no discernible density anomaly and while salinities within the plume are generally lower, their values fall within the distribution of background values making the use of initial mixing lines impractical. Dilution values obtained with the CDOM proxy in AUV monitoring missions do not have the same constraints as previous methods.

Once the plume characteristics have been identified in CDOM and salinity, samples falling within given thresholds identifying the water mass can be plotted to show the spatial distribution of the plume (Figure 24). The horizontal spatial distribution shows the August 3, 2010 plume advecting toward the southeast as far as sampling was conducted (5 km), while the vertical distribution shows the core of the plume centered at 62 m and a minimum rise height depth of 45 m. The spatial distribution of the February 25, 2011 PLOO plume is determined by selecting samples specific to the plume, in this case CDOM values greater than or equal to 4.3 ppb and salinity values less than or equal to 33.65 ppt (Figure 24b). The maximum REMUS depth was extended to 90 m for the February 25, 2011 monitoring mission which enabled mapping of the entire vertical structure of the plume with its core centered at 67 m and rising to a minimum depth of approximately 50 m. The horizontal distribution of the plume is strongly correlated with the estimated current trajectories based on the PLOO buoy velocity profile.

PLOO plume distributions based on water-mass characteristics in salinity and CDOM for all monitoring missions are presented in Figures 25 and 26. In all cases, there is good agreement between the estimated plume trajectory based on velocities measured by the buoy and the observed plume distribution. The horizontal distribution is much denser for missions near the diffuser (e.g. February 25, 2011 through April 22, 2011) while the distribution in the far-field

missions was sparser due to the resolution of the measurements. For the January 28, 2011 and February 8, 2011 monitoring missions, the higher velocity flow fields caused an advecting plume nearer to the bottom. The observations of these plumes were limited due to the AUV's maximum running depth of 80 m. The maximum operating depth was changed to 90 m for the remainder of the missions (February 25, 2011 through April 22, 2011) which consistently captured the full profile of the plume.

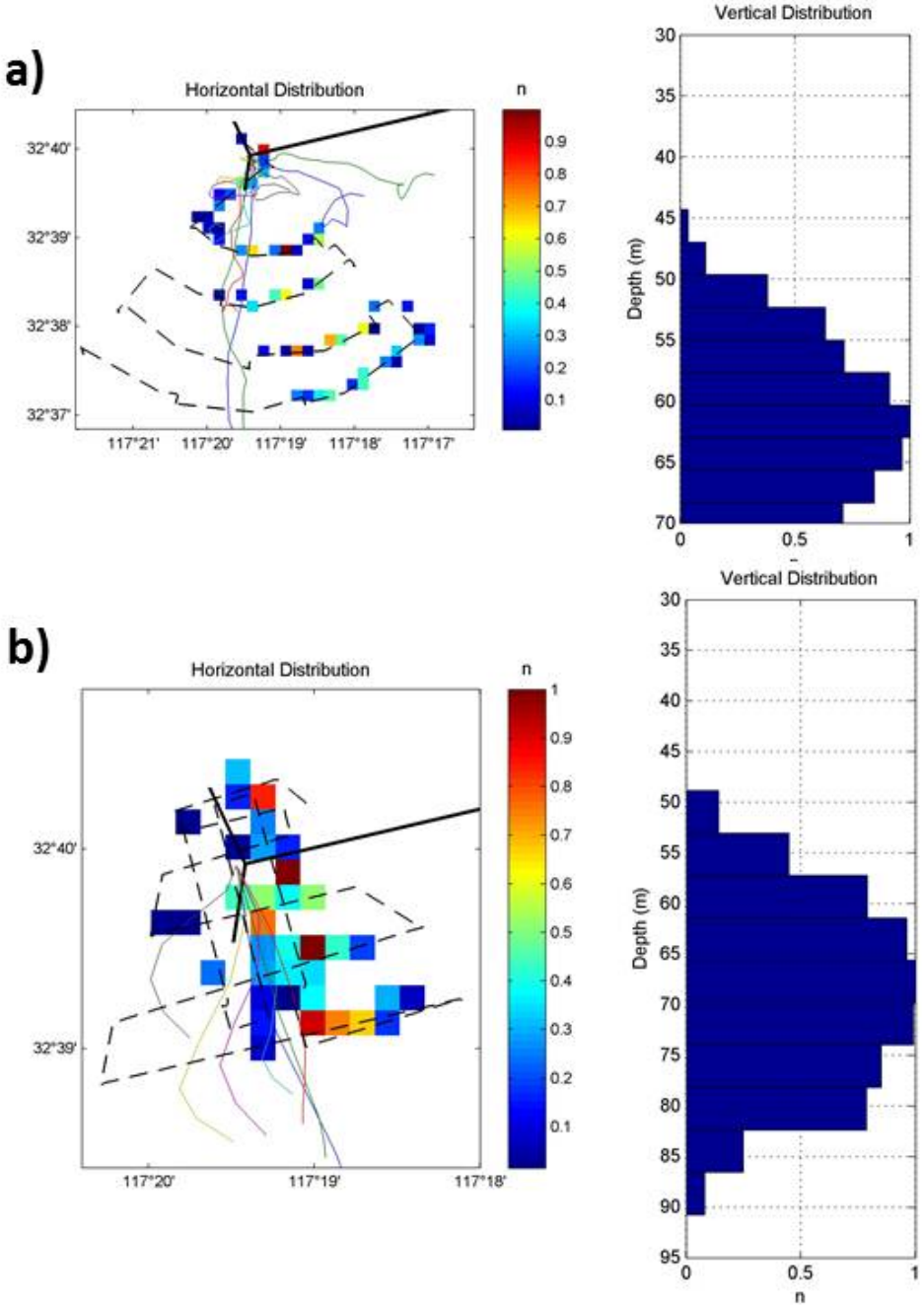

Figure 24. Horizontal (left) and vertical (right) distributions of the PLOO plume measured on August 3, 2010 (a) and February 25, 2011(b). Plume distributions are based on the number of samples with CDOM > 4.3 ppb and salinity < 33.65 ppt falling within each spatial bin (50 x 50 m horizontally and 1 m vertically) then normalized by the maximum number of samples observed in a single bin. On the horizontal distribution plot, the REMUS mission path is shown as a dotted black line, the estimated plume trajectory based on buoy velocity measurements are shown by colored lines and the PLOO outfall is shown in black.

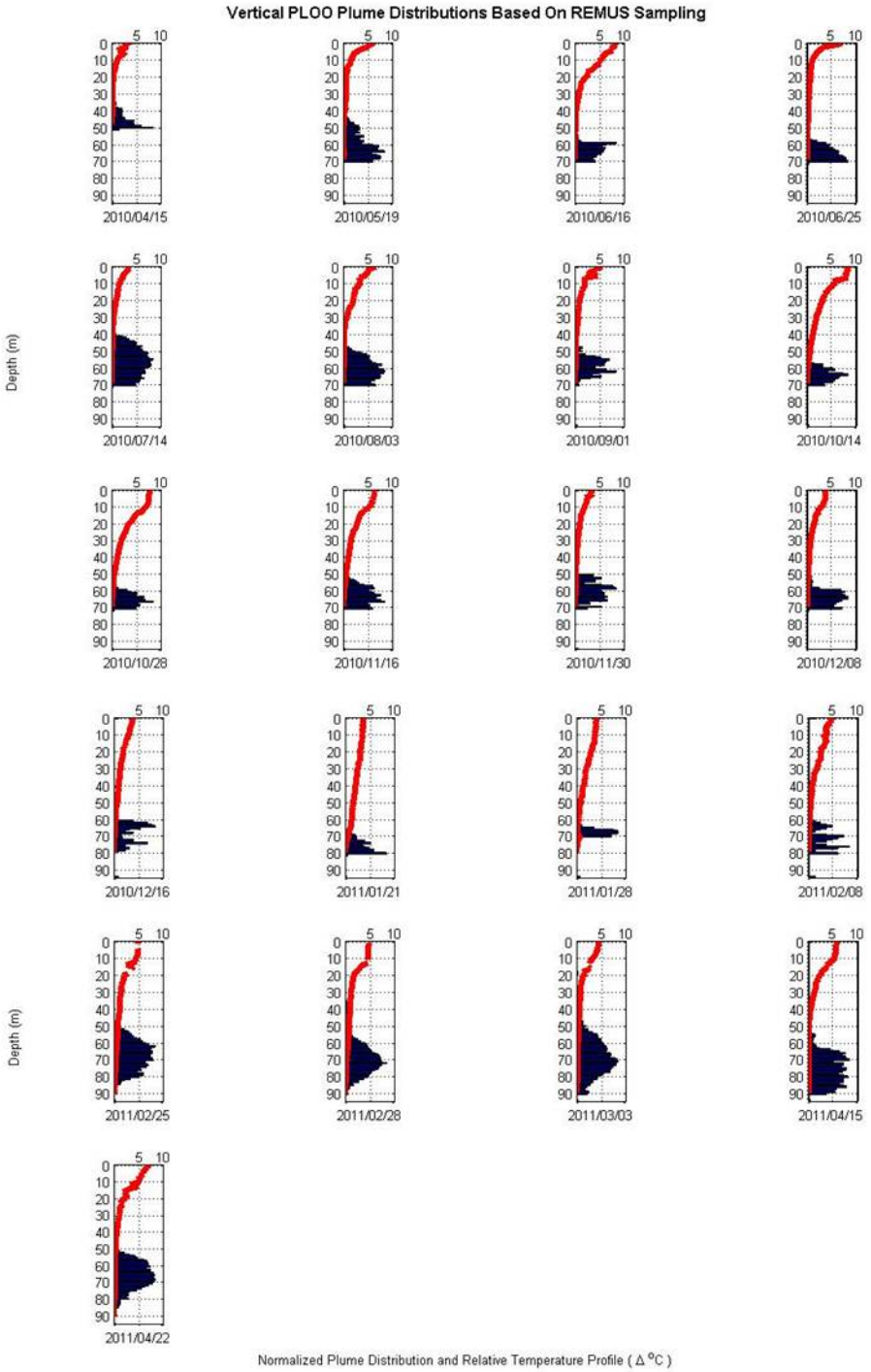

Figure 25. Plume distributions are based on the number of samples with characteristic CDOM and salinity values within 1 meter vertical bins. The number of samples is then normalized by the maximum number of samples observed in a single bin for each mission. The relative temperature profile (temperature profile relative to bottom water temperature) is plotted in red.

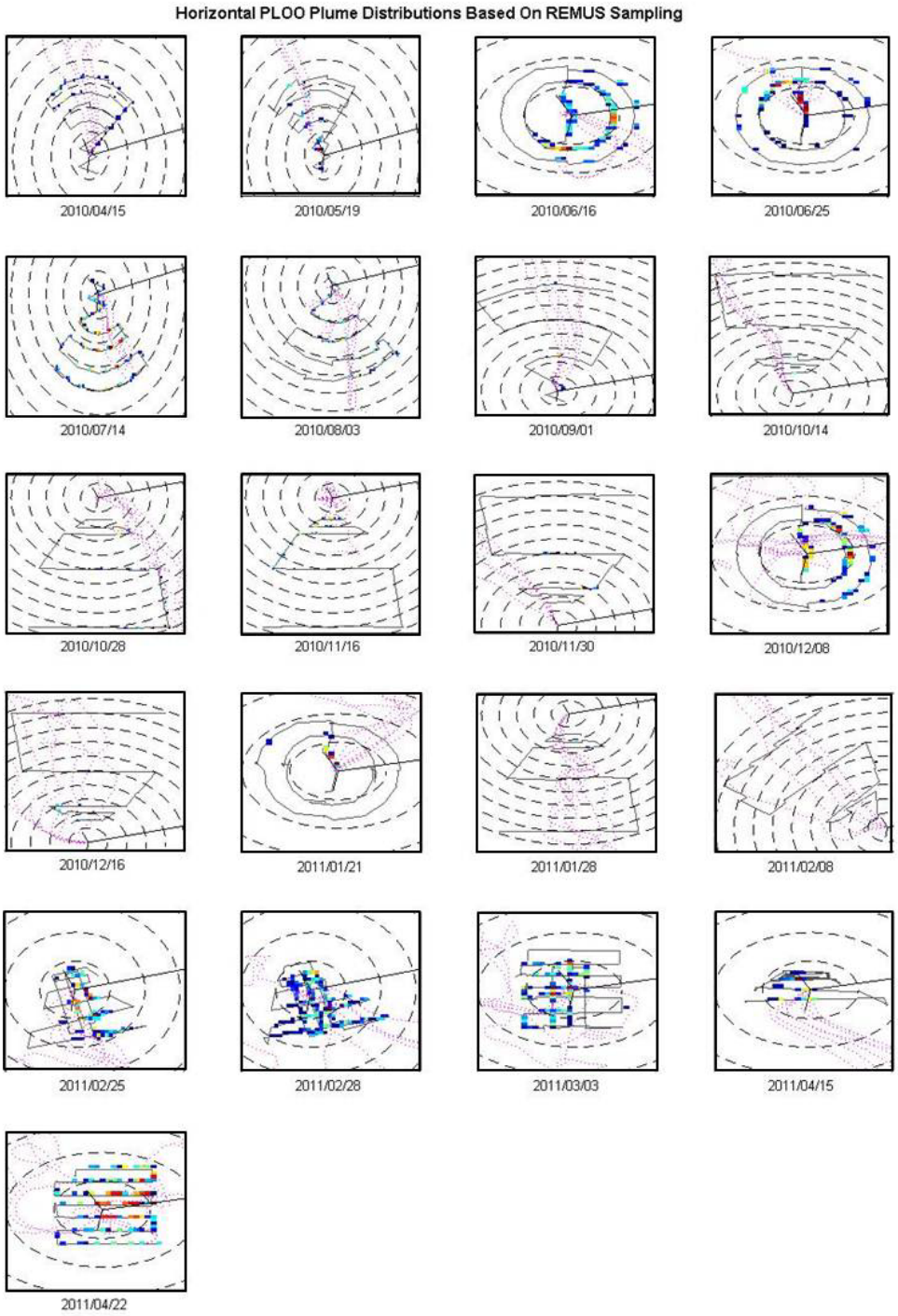

Figure 26. Plume distributions are based on the number of samples with characteristic CDOM and salinity values within spatial bins of 50 x 50 meters. The number of samples is then normalized by the maximum number of samples observed in a single bin for each mission. The REMUS mission path is shown in grey, the estimated plume trajectory based on buoy velocity measurements is shown in pink dashed lines and the PLOO outfall wye is shown in black.

2. Observed PLOO Plume Characteristics

Observed plume characteristics for each PLOO monitoring mission include plume rise height, thickness, width, and dilution. Observed plume rise height of each monitoring mission is compared to the predicted rise height in Figure 27. From April 2010 to April 2011, a minimum observed plume rise height to a depth of 35 m is observed during the February 28, 2011 mission. The observed plume rise height generally fluctuates between 40 – 60 m in depth. All observed plume rise height depths are listed in Table 7. **During the PLOO study, no surfacing events were predicted or observed due to the extreme depth of discharge**.

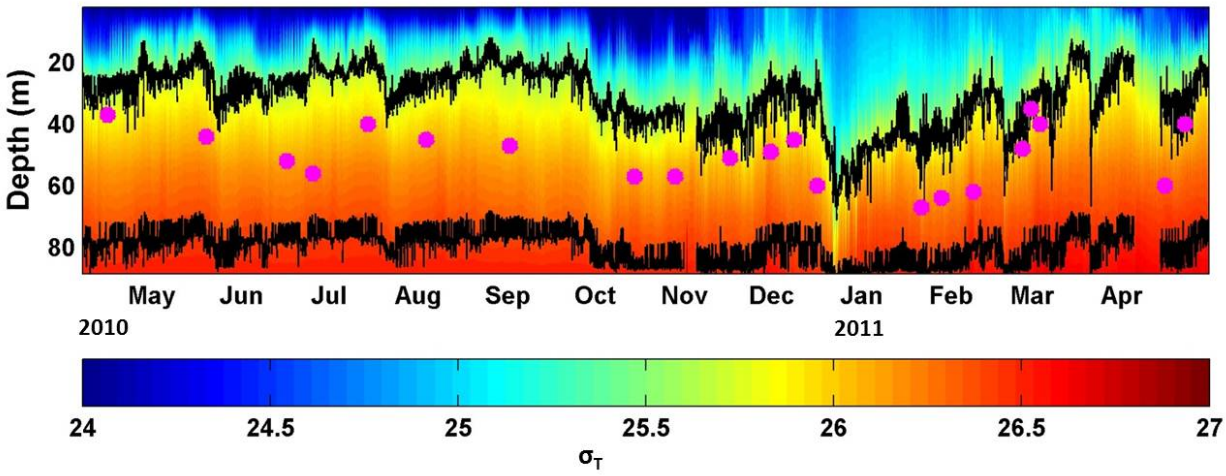

Figure 27. Density structure at the PLOO from April 2010 to April 2011. Also shown are the rise height and plume base estimated using the NRFIELD buoyant plume model. The estimated time-dependent depth extents of the plume are bound by these two black lines. No surfacing events were evident.

Velocity differences between missions explain differences observed in plume dilution and structure. Changes in plume structure and property distributions due to the increased current speed u may be parameterized by changes in the Froude number (F), defined as:

$$F = \frac{u^3}{b} \qquad \text{(Eq. 2)}$$

where u is the current speed and b is the flux of buoyancy per unit length of diffuser, or buoyancy flux, equal to $g(\frac{\Delta\rho}{\rho})(\frac{Q}{l})$ where g is the acceleration due to gravity, $\Delta\rho$ is the density difference between the plume water and seawater, ρ is the ambient seawater density at the diffuser depth, Q is the discharge flow rate, and l the diffuser length. This nondimensional parameter compares the competing effects of the ambient current to disperse and mix the plume (high Fr) with that of the buoyancy flux to concentrate and maintain the plume (low Fr) (Fischer et al. 1979; Roberts 1977; Washburn et al. 1992).

Elevated CDOM levels within the plume were used to calculate dilution values for each mission (eq. 1). Table 7 lists the average minimum dilution value of each mission and its corresponding Froude number. Higher current regimes increase the mixing between the discharge and its receiving waters causing increased levels of dilution. This is evident during the October 14, 2010, November 30, 2010, February 25, 2011, and April 15, 2011 missions with observed dilution values of 1:192, 1:304, 1:228, and 1: 204 respectively. Conversely, low current regimes account for the highest observed dilution levels of 1:117, 1:103, and 1: 109 for November 16, 2010, February 28, 2011, and March 3, 2011 missions respectively.

Table 7. REMUS survey summary including Froude number, minimum observed plume depth, and minimum observed dilution.

Date	Froude Number *	Min Observed Plume Depth (m)	Min Observed Dilution (1:N)
2010/04/15	**0.245**	37	141
2010/05/19	**1**	44	188
2010/06/16	**0.71**	52	177
2010/06/25	**0.71**	56	110
2010/07/14	**0.71**	40	125
2010/08/03	**0.245**	45	127
2010/09/01	**0.71**	47	193
2010/10/14	**3.45**	57	192
2010/10/28	**1.23**	57	184
2010/11/16	**0.09**	51	117
2010/11/30	**2.41**	50	304
2010/12/08	**0.52**	50	161
2010/12/16	**0.09**	60	248
2011/01/21	**1.57**	67	160
2011/01/28	**2.41**	64	162
2011/02/08	**1.23**	62	N/A
2011/02/25	**2.93**	58	228
2011/02/28	**0.02**	35	103
2011/03/03	**0.02**	45	109
2011/04/15	**2.41**	57	204
2011/04/22	**0.245**	50	157

* Average Froude number at depths of 60 - 90m

IV. DISCUSSION

A. Example AUV Missions

Our ability to synoptically evaluate the 3-dimensional spatial extent and hydrodynamic mixing of the plume during different seasonal conditions is best exemplified by presenting data from surveys conducted on August 3, 2010 and February 25, 2011. Plume mixing and its geometric evolution for each mission are illustrated by cross-sections of dilution at successive distances from the discharge (Figure 28a). To help delineate the contours, dilution values above 400 are not plotted.

The average velocity in the lower water column for the August 3, 2010 mission was 0.07 m/s, more than half of the average velocity estimated for the February 25, 2011 mission (0.16 m/s) yielding Froude numbers of 0.24 and 2.93 respectively (Table 8). The higher velocity current enhances near-field mixing and forms a narrow plume (Figure 28b) as it advects downstream with a width of 1.2 km at the last cross-section (1.5 km from the wye). Conversely, the plume shown in Figure 28a, dispersed by a low current regime is less mixed as it advects downstream and has a width of approximately 3 km. The differences in plume characteristics of each mission were compared at the 2 km cross-section (Figure 28a) and 1.5 km cross-section (Figure 28b) which were approximately co-located. In a parallel current (same direction as the outfall diffusers), the initial lateral plume spreads by a density current unrelated to turbulent diffusion [*Hunt et al*., 2010]. From laboratory experiments, it is predicted that the plume will spread linearly, in a V-shape according to:

$$\frac{w}{x} = 0.7F^{-1/3} \qquad \text{(Eq. 3)}$$

where w is the plume width at distance x from the source [*Roberts et al*., 1989]. Characteristics discussed in this section are summarized in Table 8. Equation 3 predicts a plume width of 2.8 km and 1.1 km for the co-located cross-sections of the August 3, 2010 and February 25, 2011 missions respectively; comparing well with measured values. We note that equation 3 was developed from straight-line diffuser tests, however the large angle (152 degrees) between the y-shaped diffusers located at PLOO make this a reasonable assumption for evaluating trends.

B. Far-Field Mixing

Plume models can reasonably predict bulk plume properties such as equilibrium depth, thickness, and dilution in the near-field. However, current plume models cannot accurately represent plume complexity, particularly the patchy nature of the wastefield [*Ramos et al*., 2005] and the role of oceanic turbulence in mixing the plume. The NRFIELD model assumes a uniform current, i.e., the current is constant in speed and direction over the rise height, however vertical shear in coastal currents will have potential to influence plume evolution. For the PLOO, currents are found to have significant vertical shear and temporal variability which introduces complexity in developing the sampling plan to efficiently track the plume from the near-field to the far-field; placing a requirement on environmental adaptation.

The importance of monitoring plume waters into the far-field is evident in the plume cross-sections depicted in Figure 28. Dilution of the plume in the far-field for a majority of the monitoring missions at the PLOO looked similar to the August 3, 2010 mission (Figure 28a) where mixing occurred slowly as distance increased from the diffuser. This result is expected since mixing in the far-field is due to background ocean turbulence, which typically produces much slower mixing than that in the near-field which is governed by buoyancy and momentum exchange processes from the diffuser jet. However, vigorous mixing in the far-field was observed in the February 25, 2011 monitoring mission (Figure 28b). As the plume progressed from the 0.25 km cross-section to the 1.5 km cross-section, the plume becomes virtually undetectable below a depth of 65 m, indicating significant mixing over the 1.25 km distance. In comparison to Figure 28a, the dilution only increased from 130 to 184 over a distance of 4 km. Figure 28b also shows an additional rise of the plume of approximately 10 m from a height of 60 m in the 0.25 km cross-section to 50 m at the 0.75 km and 1.5 km cross-sections.

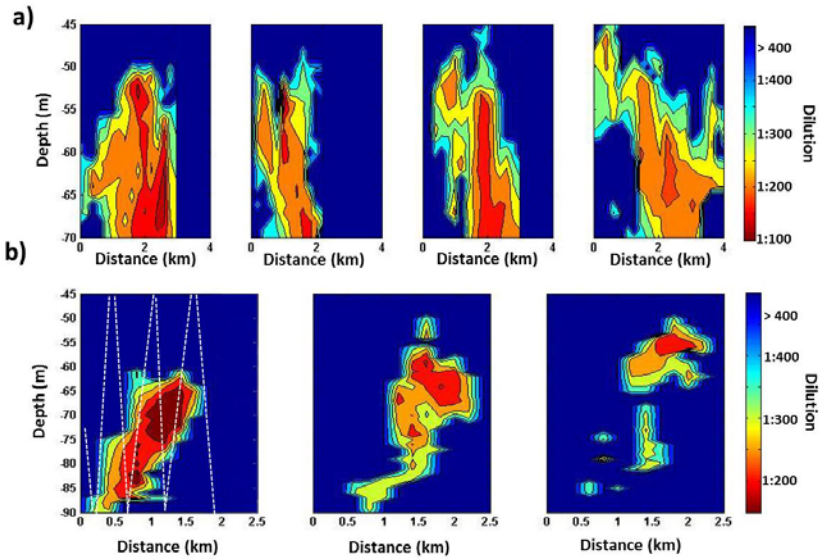

Figure 28. Cross-sectional dilution plots as a function of range from the outfall for (a) August 3, 2010 and (b) February 25, 2011 monitoring missions. The range is measured from the wye to each successive cross-section; (a) 2 km, 3 km, 4 km, 5 km and (b) 0.25 km, 0.75 km, 1.5 km. The figures show the distribution of the plume width and thickness as it progresses downstream. The sawtooth REMUS pattern is included in the 0.25 km cross-section, Figure 28b.

Table 8. Comparison of 8/3/2010 and 2/25/2011 background conditions and their effect on plume width.

Parameter	8/3/2010	2/25/2011
Average Current Velocity (m/s)	0.07	0.16
Froude number (F)	0.24	2.93
Plume width (km) *	3	1.2

* Measured at the 2 km cross-section (8/3/2010) and the 1.5 km cross-section (2/25/2011)

C. Computing Plume Dispersion

The cross-sectional plots shown in Figure 28b were used to estimate horizontal dispersion of the February 25, 2011 plume. Linear growth of the transverse dimension (x) of the plume over time (t), as measured from the contour plots, was used to estimate the bulk diffusivity coefficient K_x. Employing the methods described in *Elliott et al*. [1997], the plume distribution was assumed to be Gaussian in shape where K_x is related to the variance (σ_x^2) of the Gaussian-shaped relationship between concentration and the length scale:

$$\sigma_x^2 = 2K_x t \qquad \text{(Eq. 4)}$$

The method, more recently used to estimate horizontal dispersion for an oil transport model in *French-McCay et al*, [2007], assumes that a 4σ approximation of the length scale provides a realistic estimate of patch width. Therefore, the standard deviation (σ) was computed for each cross-section shown in Figure 28b. It was assumed that the plume at the 0.25 km cross-section was fully formed even though it is not located at the end of the diffuser. However, any difference in initial plume width from this point and the end of the diffuser will have a negligible effect on dispersion calculations.

The variance (σ^2) was plotted against diffusion time, and least squares was used to determine the value of the transverse diffusion coefficient K_x . Based on the three cross-sections seen in Figure 28b, K_x = 2.35 m^2/s (standard error = 0.77). This result falls in the range predicted by *Okubo* [1971] of 1-10 m^2/s for length scales of 1-10 km. The diffusion coefficient is commonly assumed to be related to the plume width (L) according to the "4/3" power law [*Hunt et al*., 2010]:

$$K_x = \propto L^{4/3} \qquad \text{(Eq. 5)}$$

where $\propto$ is a constant with typical values between 0.002 to 0.01 $cm^{2/3}/s$ for oceanic diffusion [*Fischer et al*., 1979]. Assuming an initial field width L of 1.2 km (from Figure 28b, 0.25 km cross-section), yields $\propto$ = 0.004.

A solution to the problem of horizontal turbulent diffusion from a finite line source in a uniform current is derived by *Brooks* [1960]. The solution ignores the effects of vertical diffusion and longitudinal dispersion; both are typically small when compared to their horizontal and transverse counterparts. Based on the 4/3 law, the resulting equation is:

$$\frac{c_{max}}{c_0} = \left[\text{erf}\left(\frac{3/2}{\left(1+8\propto L^{-2/3}t\right)^3-1}\right)^{\frac{1}{2}}\right]^{-1} \qquad \text{(Eq. 6)}$$

where erf is the standard error function, c_{max} is the maximum concentration at time (t), and c_0 is initial concentration. The ratio c_{max}/c_0 can be interpreted as the further dilution obtainable due to transverse diffusion in the far field during advective transport for a time t. For the February 25, 2011 mission, L = 120,000 cm, $\propto$ = 0.004, and an estimated travel time of 3 hours (10,800 s) to 1.5 km cross-section (based on t = x/U where x is distance from source and U is current velocity), yielding c_{max}/c_0= 1.01. Thus, we would expect the minimum dilution observed at the 0.25 km cross-section (Figure 28b) of 145 to increase only slightly to 147. However, our

observations reveal a significant increase of dilution from 145 at the 0.25 km cross-section to 232 at the 1.5 km cross-section. While, equation 6 should be used conservatively due to the assumptions of this solution [*Koh and Brooks,* 1975], such a large difference between predicted and measured dilutions implies that turbulent mixing is occurring leading to this increase in dilution.

D. Near- and Far-field Trends

Figure 29 presents the median of the dilution ratios for all missions that exhibited steady current regimes parallel to the diffusers (North/South). The median of the dilution ratio is based upon all the data sampled by the AUV both in the near and far-field at a particular range pass. The time estimates are based upon the advection time scale as computed from the current meter data. Higher current regimes (Fr > 0.11) were denoted by solid asterisks, while lower current regimes (Fr < 0.11) were denoted by hollow circles. The analysis indicates that the plume rapidly mixes in the near-field at an effective rate of t^2 before quickly adjusting to a slower rate of $\sim t^{1/10}$ in the far-field. The trend in the far-field is independent of current velocity as illustrated by each trendline at different Fr numbers. The rapid transition to slow mixing after initial mixing is expected since dilution in the far-field is dominated by lower background ocean turbulence levels compared to the near-field jet where buoyancy and momentum exchange processes dominate. Figure 29 illustrates both the dynamic range of discharge plume dilutions over which CDOM can be used as well as the effectiveness of the AUV sampling to characterize both near-field and far-field mixing.

Taylor's [1953, 1954] landmark papers on shear dispersion predicts tracer variance will grow linearly with time after an initial adjustment period, however, *Okubo* [1971], using the data from horizontal diffusion tracer experiments obtained prior to 1971, created diffusion diagrams for a time scale of diffusion between 2 hours and 1 month that indicated non-Fickian diffusion or a non-linear growth in variance with time. The observed plume characteristics used to compute median dilutions (Figure 29) also show this non-linear trend.

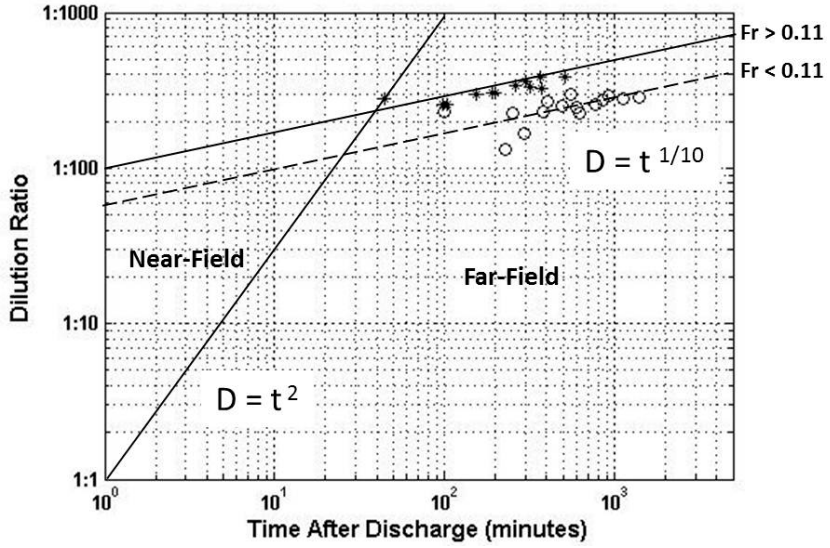

Figure 29. Median measured dilution ratios using the CDOM proxy as a function of time from PLOO. Data from missions with steady currents that were parallel to the diffusers (North/South) were combined to show the log-log trend in dilution as a function of time from the outfall. The trend based on missions performed in high Fr number regimes (defined as Fr > 0.11) compared to low Fr number regimes (F < 0.11) is also shown.

E. Comparison with Analytical Mixing Model

The observed dilution, plume thickness and height are compared with predictions made by the NRFIELD plume model and presented in Table 9. The data used for this comparison are the observed values measured at what was estimated to be the end of the near-field zone as characterized by the plume reaching its equilibrium depth. The August 3, 2010 mission was designed to track the plume in the far-field to a range of 5 km. Table 9 shows measured plume characteristics as estimated from Figure 28 compared with the NRFIELD predicted values. The plume thickness given in Table 9 is an estimated range as the vehicle surveyed to 70 m while the discharge originates at 90 m. The model predicts a dilution of 238 while dilution calculated from the average of the observed maximum values is 130. The same pattern holds for the February 25, 2011 mission with predicted dilution at the end of the near-field at 300 and observed at 206. Dilution values computed at increasing distances from the diffuser remained significantly less than NRFIELD predicted dilution values, leading us to believe the differences are not a result of misidentifying the boundary of the near-field mixing zone.

A 3-month analysis of the CDOM variability of the source effluent at the PLWTP provided a range of approximately +/- 15 ppb of the CDOM constant (121 ppb) used to calculate dilutions. These differences will not produce significant errors in the dilution calculations. Another potential explanation for the dilution mismatch may be a limitation of the model's parameterization of dilution as a function of Froude number (e.g. $D \sim u^{1/2}$) in addition to the assumptions of the discharge occurring in a uniform/constant current. For example, the model's predicted dilution will vary significantly across inputs ranging from 1-5 cm/s while natural variability of coastal currents can be an order of magnitude larger. In addition, to the challenges of going from laboratory to full-scale, the difference in dilutions may also be partially explained

by the mismatch between the discrete measurements provided by the AUV and the inherent spatial averaging implicit in the model output. However, it is unlikely that these sources of errors would account for the total difference between predicted and observed dilution values seen in Table 8.

The NRFIELD model assumes the submerged wastefield resulting from multi-port line diffusers forms a line plume in which individual plumes from each diffuser port merge before the terminal rise height [*Roberts et al*., 1989]. For the PLOO, the ratio of the port spacing to rise height is large, thus the diffuser port plumes do not fully merge before the terminal rise height, creating a point plume. The work of *Tian et al*., [2004] developed semi-empirical equations to predict the major near-field characteristics, including dilution of a submerged plume. However, they found that their results were not widely applicable for prediction of near-field dilution for a point plume, which suggests that the equations governing dilution of a line plume may not be practical for a point plume. Consequently, it is feasible that the NRFIELD line plume assumption could lead to the discrepancies between predicted and observed dilution at the PLOO [*P. Roberts*, personal communication].

Table 9. Comparison of REMUS field measurements and NRFIELD predictions for 8/3/2010 and 2/25/2011.

	8/3/2010		2/25/2011	
Parameter	**Measured**	**Predicted**	**Measured**	**Predicted**
Near-field dilution	130*	238	206*	300
Height of minimum dilution (m)	26	26.8	23	22.9
Plume thickness (m)	25-30	27.2	23	23.4
Plume height (m)	44	63	48	61

* Based on observations nearest to the end of the initial mixing zone.

F. Enhanced Far-Field Mixing and Plume Rise

The mechanism of the enhanced mixing and the additional plume rise illustrated in Figure 28b is not immediately evident. Analysis of the source effluent density prior to discharge did not reveal any significant differences. The NRFIELD model predicts the end of the near-field at 112 m from the effluent source while the first cross-section is located approximately 0.25 km from the source, thus minimal additional mixing or plume rise is expected beyond this point without an external mechanism. The dominant mechanism for converting fluid motion to mixing in the stratified ocean is shear instability in which shear overcomes the stability of stratification [*Geyer et al*., 2010]. A Richardson number ($Ri = N^2/S^2$, where N is the buoyancy frequency and S is the vertical shear) less than 0.25 is typically used as a critical value in which shear-related instabilities are thought to occur for a linearly varying current and density. *Abarbael et al*. [1984] included nonlinear interactions and concluded $Ri < 1$ is sufficient for instabilities to occur, while *Mack and Schoeberlein* [2004] found strong evidence of shear instabilities during high resolution tow measurements, but no critical Ri, rather a range from 1.3 to less than 0.25 that typically coincided with observed mixing.

Ri profiles were calculated along the horizontal AUV path using the current velocity observations from the buoy ADCP and AUV density observations, then compared with current velocity and shear (Figure 30). The February 25, 2011 mission experienced significantly higher current velocities than the August 3, 2010 mission. Friction with the seafloor caused adjacent velocities to slow creating the Bottom Boundary Layer (BBL) between the depths of 80 - 90 m for the higher velocity February 25, 2011 mission. The resulting low Ri number due to the increased shear implies turbulent mixing is likely occurring in the BBL. Several depths above the BBL also show a drop in the Ri number below its critical threshold of 1, most notably between 50 - 60 m. Changes in these regions are caused by decreased buoyancy frequency due to variations in the density field. Comparatively, the Ri number for the lower current regime observed by the August 3, 2010 mission did not drop below the critical value of 1 at any depth.

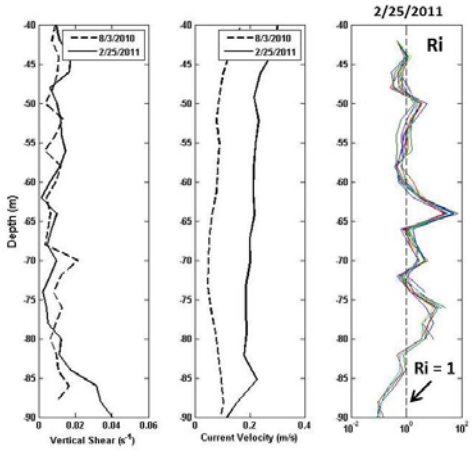

Figure 30. Profile plots of velocity shear and current velocity for August 3, 2010 (dotted line) and February 25, 2011 monitoring missions. The Ri profile plots of from the area of enhanced mixing seen in Figure 19b.

Closer examination of the statistics of the depth of the measured plume, the local salinity and temperature profile (REMUS measurements), and the Ri number profiles (Figure 30) gives a clue to the mechanism causing the additional plume rise and enhanced mixing. The bar graph shows the normalized plume density versus depth at the 0.25 km (hollow bars) and 1.5 km (solid bars) cross-sections. Since these cross-sections are beyond the initial mixing zone (near-field) and at their equilibrium height, the plume is not expected to rise and mix significantly without external influence. However, Figure 31 clearly illustrates an additional rise of 10 m over a distance of 1.25 km while Figure 28b shows significant mixing continues to occur beyond the initial-mixing zone. The temperature profile shows a temperature fluctuation between the depths of 50 - 55 m. The salinity profile also shows a small fluctuation from approximately 52 - 58 m. Observed isotherms from the buoy temperature chain at depths of 2 m, 31 m, and 55 m were analysed to determine the temporal temperature fluctuations in the region (Figure 32). The isotherms show significant temperature variations starting around February 19, 2011 and persisting through the February 25, 2011 monitoring mission. These variations are indicative of large amplitude internal waves propagating through the study area [*Phillips*, 1997].

Linear (small amplitude) and nonlinear (amplitude is a large fraction of the water depth) waves are prevalent features of coastal circulation in the region surrounding the PLOO [*Lennert-Cody and Franks*, 1999]. *Petrenko et al.,* [2000] was the first to show the influence of internal waves on an effluent plume. The Sand Island wastewater plume was shown to follow the vertical displacements of isotherms generated by a semi-diurnal internal tide. The authors found that displacements of 40 m yielded internal tides of the order of 15 m. Similarly, the isotherm displacements observed in this study after February 19, 2011 suggest internal waves with amplitudes between 10 to 15 m are present in the study area. For comparison, isotherms during the August 3, 2010 monitoring mission (Figure 32b) show no indication of internal wave activity which explains the plume's behaviour illustrated in Figure 28a (little additional mixing, no vertical displacement).

There is no shortage of proposed mechanisms capable of generating internal waves, including surface generation by the atmosphere through travelling pressure fields, variable buoyancy flux, or variable wind stress with the latter being most plausible; internal generation through the process of decay of large-scale circulations and mesoscale eddies by breaking or baroclinic instability; and bottom generation through interaction of the quasisteady currents advecting in a stratified ocean over bottom topography (lee waves) [*Thorpe*, 1975; *Garrett and Munk*, 1979]. In the PLOO region, the internal waves form as the tide moves over rough bottom topography offshore generating significant vertical shear of the horizontal currents through the water column. In shallow water the waves lose energy and can break causing vertical mixing [*Pineda*, 1994].

Based on the analysis presented in this section, a nonlinear internal wave generated by on-shore tidal flow over rough bottom topography is the most likely mechanism behind the enhanced mixing and vertical rise of the plume observed in Figure 28b. It is evident that vertical isothermal (and corresponding isopycnal) oscillations have a strong influence on the plume's mixing and position within the water column. Omission of the processes governing these variations is another possible source of discrepancies between in-situ observations and plume models results (*Petrenko et al*., 2000].

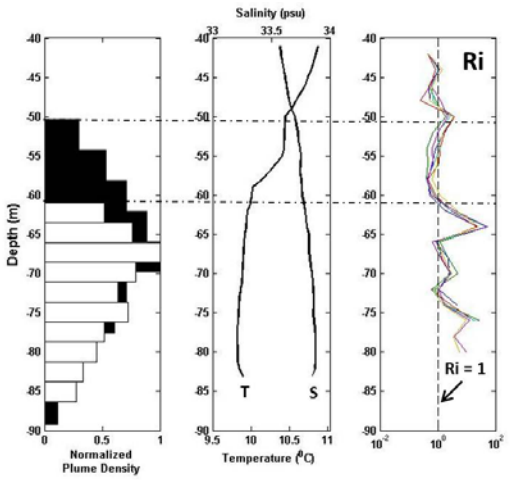

Figure 31. Normalized plume density plotted against depth for the 0.25 km cross-section (hollow bars) and the 1.5 km cross-section (black bars) illustrating a rise in plume height of 10 m in the far-field and profile plots of temperature, salinity and Ri number in the area of interest.

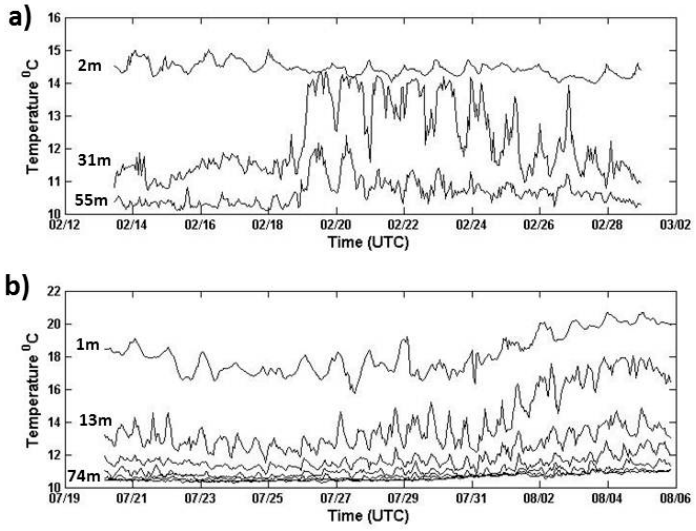

Figure 32. Observed isotherms at depths of (a) 2 m, 31 m, and 55 m from February 13, 2011 to February 29, 2011 and (b) 1 m, 13 m, 25 m, 38 m, 50 m, 62 m and 74 m from 20 July 2010 to 6 August 2010.

Internal waves also affected the PLOO study area beginning on December 22, 2010 and lasting for several days (Figure 33). The event was the maximum observed temporal temperature variability within the water column from April 2010 to April 2011 and suggests the presence of a large amplitude internal wave. The isotherms suggest the internal wave is significantly larger than the one illustrated in Figure 32 due to the temperature fluctuations at deeper depths. The sustained northwest current direction during the December 22, 2010 event was different than all other internal wave events throughout the PLOO study which suggests a different mechanism generated the observed internal waves. Figure 34a shows a 10-hour average profile plot of the currents on December 22, 2010. The currents are uniform in direction throughout the water column and have an average magnitude of 35 cm/s between the depths of 60 m and the surface. If these current conditions persist to the south, the northwesterly currents would intersect with the Coronado Islands before reaching the PLOO study area (Figure 34b). HF radar derived surface currents confirm that the surface currents direction are the same in the South Bay as observed at PLOO (Figure 35). If we assume that the current directions are also uniform with depth in the South Bay, we can conclude that the most plausible mechanism of the large amplitude non-linear internal waves observed at PLOO on December 22, 2010 is caused by the interaction of the currents with the Coronado Islands.

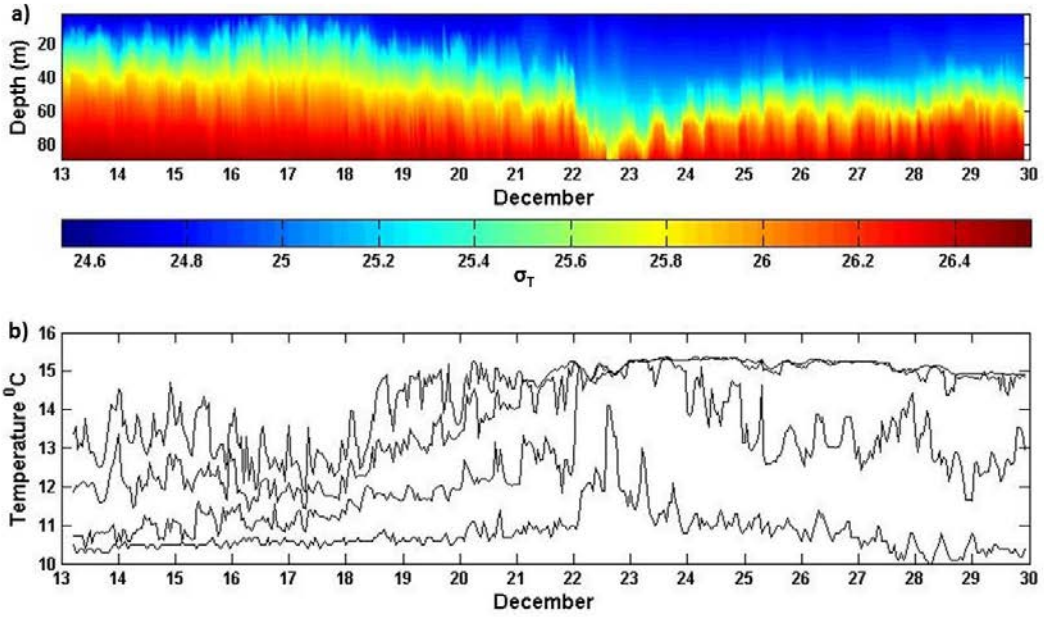

Figure 33. (a) Ocean temperature time series from December 13, 2010 to December 30, 2010. (b) Observed isotherms at depths of 19 m, 31 m, 54 m, 89 m from December 13, 2010 to December 30, 2010 .

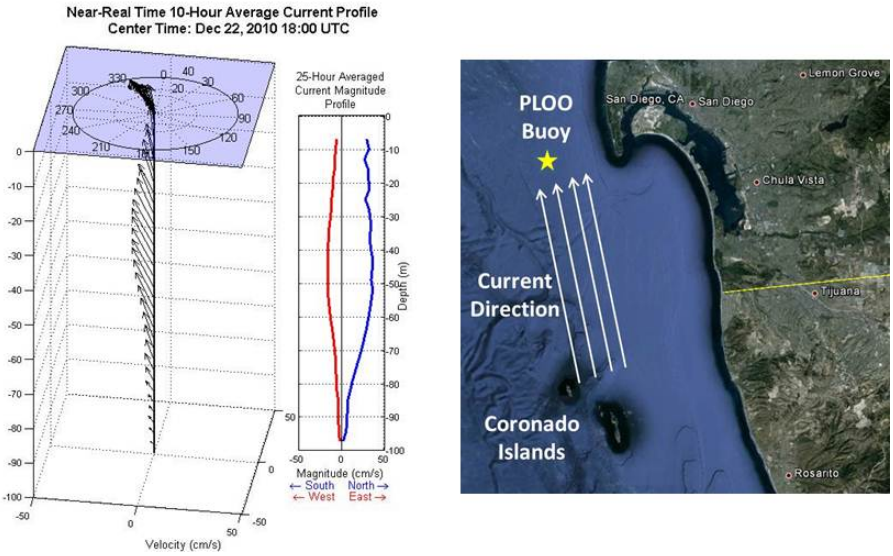

Figure 34. Uniform alongshore current direction that intersects the Coronado Islands and affects the PLOO study area on December 22, 2010.

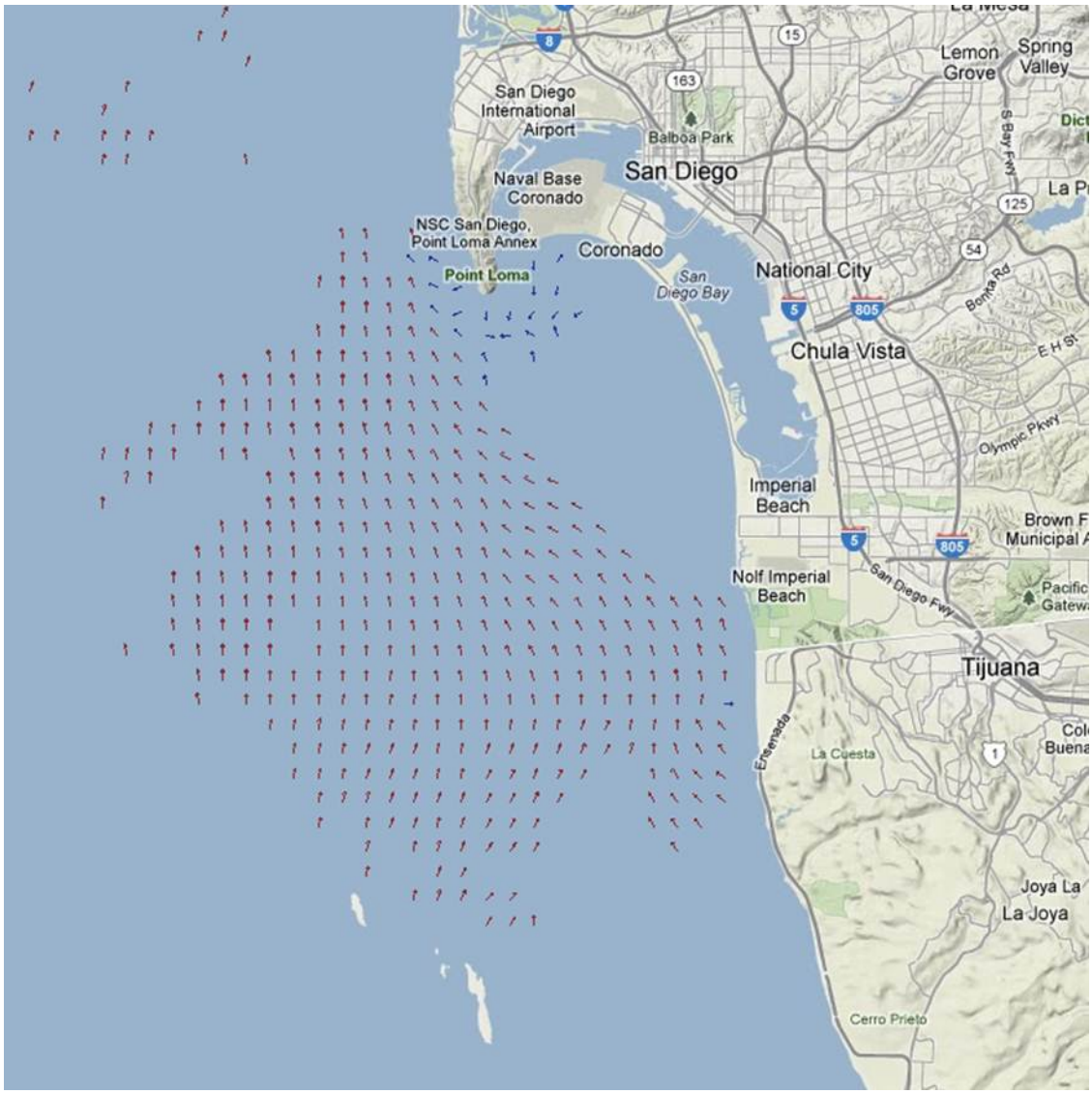

Figure 35. Online display of HF Radar derived surface currents in the South Bay on December 22, 2010. Sites maintained through this effort include Point Loma, Border Field State Park, and Coronado Islands.

V. CONCLUSIONS

Despite the political, ecosystem, and public health interests in coastal water quality, ocean monitoring of the physics responsible for the transport of a land-based or offshore wastewater discharge plume is difficult. Water quality sampling required of an NPDES permit holder in the receiving waters of their discharge typically is designed for assessing water quality on a statistical basis, not for assessing the fate and transport of their discharge. **The sampling required of an NPDES permit provides snapshots of ocean conditions, but under-samples the ocean in the time and space domains that are necessary to estimate the position of the plume.** In addition, the transport and orientation of discharge plumes are highly variable because

of ocean dynamics and can be elusive to track using a fixed grid of boat-based sampling stations. As a result, assessment of station data is often inconclusive. One reason sampling protocols for monitoring receiving water have not evolved significantly over the years is the lack of available tools that can provide appropriate monitoring at the appropriate scales required to accurately estimate the fate and transport of the discharge plume. Methods using vessel-based sampling at fixed grid sampling stations in the receiving waters have not changed significantly in 30 years.

A. Findings

Analysis of the data from this study has resulted in the following findings:

1. Measurements of ocean stratification at the PLOO and subsequent modeling of the behavior of the buoyant plume rise height, estimated that the discharge plume did not surface during the 12-month telemetry mooring monitoring period. The most likely mechanism that could cause the plume to surface would be a strong upwelling event, however the plume was never observed or predicted to rise to the surface even during such upwelling conditions. Thus, due to the deepwater depth of the discharge (~100m) and typical stratification conditions during the wet and dry seasons, it is unlikely oceanographic conditions at PLOO will be favorable for a surfacing plume.

2. The NRFIELD model predicts the PLOO plume to rise through the weakly stratified bottom layer until it intersects with the strongly stratified upper layer. A range of rise heights between the depths of 20-30 m was common during the months of April 2010 to October 2010, while warm waters extended to a depth of 30 m from October 2010 through November 2010 causing stronger stratification at these depths which suppressed the predicted rise height to a depth of approximately 40 m. For all monitoring missions, the observed plume rise height remained below the predicted rise height and generally fluctuated between 40 – 60 m in depth. The maximum observed rise height occurred during the February 28, 2011 monitoring mission when the plume rose to a depth of 35 m.

3. Subsurface currents measured by the oceanographic mooring at the outfall discharge site can be used to estimate the transport and orientation of the PLOO subsurface plume. Generally, the plume was advected either North or South for all missions, with exceptions for the February 28, 2011 and March 3, 2011 (minimal current), April 22, 2011 (variable - changing direction in the hours preceding a mission), and the June 16, 2010 and December 8, 2010 monitoring missions in which an on-shore flow was observed.

4. The AUV using a CTD probe, along with sensors for measuring changes in the ocean's optical properties, was able to effectively map out the location of the subsurface plume. With proper vehicle configuration and mission programming, the vehicle was able to detect the plume 100 percent of the time. The ability of the vehicle to sense the subsurface plume was enabled using proper mission planning of the vehicle track and consideration of plume transport estimates using PLOO mooring data in near-real time. The plume orientation measured by the AUV matched estimated trajectories from the ocean mooring velocity profile and stratification measurements for all missions. A total of 21 sampling missions were conducted. The mean observed dilution ratio of PLOO wastewater to seawater determined from AUV CDOM measurements was 1:170. However, the mean NRFIELD

predicted dilution based on the oceanographic conditions from the PLOO mooring was 1:357. The NRFIELD model assumes the submerged wastefield resulting from multi-port line diffusers forms a line plume in which individual plumes from each diffuser port merge before the terminal rise height. For the PLOO, the ratio of the port spacing to rise height is large, thus the diffuser port plumes do not fully merge before the terminal rise height, creating a point plume. This is the most feasible explanation for the difference between observed and predicted dilutions.

5. Linear (small amplitude) and nonlinear (amplitude is a large fraction of the water depth) waves are prevalent features of coastal circulation in the region surrounding the PLOO. In the region off Pt. Loma, the internal waves form as the tide moves over rough bottom topography offshore generating significant vertical shear of the horizontal currents through the water column. In shallow water the waves lose energy and can break causing vertical mixing. The February 25, 2011 monitoring mission showed that vertical isothermal (and corresponding isopycnal) oscillations have a strong influence on the plume's mixing and position within the water column and omission of the processes governing these variations is another possible source of discrepancies between in-situ observations and plume models results.

B. Published Work

The PLOO behavior study resulted in two peer-reviewed published journal articles:

1. Rogowski, P., Terrill, E., Otero, M., Hazard, L. and Middleton, W. (2012), Mapping Ocean Outfall Plumes and their Mixing using Autonomous Underwater Vehicles. *J. of Geo. Phys. Res*., **117**, C07016.

2. Rogowski, P., Terrill, E., Otero, M., Hazard, L. and Middleton, W. (2012), Ocean Outfall Plume Characterization using an Autonomous Underwater Vehicle. *Water and Science Tech*., (in press).

VI. MONITORING RECOMMENDATIONS

As a result of the findings reported herein for the Point Loma Ocean Outfall Plume Behavior Study, a recommended set of activities is proposed to assist with future receiving waters monitoring efforts for the PLOO discharge.

1. Continued operation of an oceanographic mooring system designed to measure subsurface velocity and ocean stratification is recommended to document the state of the receiving waters into which the PLOO discharges. Measurements conducted during this study showed that the probability of the PLOO plume surfacing is minimal. However, the subsurface velocity measurements proved invaluable for estimating the location of the plume so that it could be effectively sampled. Consequently, we recommend that the NPDES-mandated quarterly water quality sampling component of the City's ocean monitoring program be modified to use telemetered ADCP/temperature data from a permanent mooring located near the terminal diffuser wye structure of the outfall (discharge site) in order to design a more adaptive and optimized sampling grid pattern for these surveys.

2. The present offshore water quality sampling grid specified in the City's NPDES permit is too coarse in space to accurately identify where the submerged PLOO plume is located. If the goals of this component of the City's monitoring program are to sample the receiving waters to measure plume location and dilution levels, it is recommended that continued usage of a mobile AUV as described herein be in place and integrated with near-real-time reports of water column stratification and subsurface velocity. The approach used for the present plume behavior study involved programming an AUV to sample the ocean in locations probable for the PLOO plume to be present. The mission programming was guided by hourly reports of stratification and subsurface velocity provided by an ocean buoy located at the wye of the outfall (see Recommendation 1). This methodology allowed for observations of the dilution and fate of the effluent to a lateral distance of over 9 km from the diffusers. Dilution levels at these extents are similar to those nearer to the diffuser since mixing in the far-field is generally a slow process governed by oceanic turbulence. If NPDES monitoring goals include determination of the fate, extent, and dilution of the plume at large distances from the diffusers, utilization of an AUV will be essential.

VII. ACKNOWLEDGMENTS

Funding for this project was provided by NOAA Award No. NA08NOS4730441 to the City of San Diego Public Utilities Department by the National Oceanic and Atmospheric Administration. The work was conducted by the Scripps Institution of Oceanography under Contract H094679 between the City and UC San Diego.

VIII. LITERATURE CITED

Abarbael, H. D., D. D. Holm, J. E. Marsden, T. Ratiu (1984), Richardson number criterion for the nonlinear stability of three dimensional stratified flow, *Phys. Rev. Lett*., 52, 2352–2355.

Baumgartner, D. J., W. E. Frick, P. J. W. Roberts, (1994), Dilution models for effluent discharges, 3rd Ed., Rep. No. EPA/600/R-94/086. Office of Research and Development, U.S. Environmental Protection Agency, Washington, D.C.

Besiktepe, S., T. E. Ozsoy, M. A. Latif (1995), Sewage outfall plume in the 2-layer channel - An example of Istanbul outfall, *Water Sci. Technol*., 32, 2, 69-75.

Bratkovich, A. (1985), Aspects of the tidal variability observed on the southern California continental shelf, *J. Phys. Oceanogr*., 15, 225-239.

Brooks, N.H. (1960), Diffusion of sewage effluent in an ocean current, presented in First International Conference on Waste Disposal in the Marine Environment, University of California, Berkeley.

Chadwick, D. B., and J. L. Largier (1999b), Tidal exchange at the bay-ocean boundary, *J. Geophys. Res.,* 104, 29901–29924.

Ekman, V.W., (1905), On the influence of the earth's rotation on ocean currents. Arkiv foer Matematik Astronomi Och Fysik (Swedish), 2: 1–52.

Elliott, A. J., A. G. Barr, D. Kennan (1997), Diffusion in Irish Coastal Waters, Estuarine, *Coastal and Shelf Science*, 44 (Supplement A), 15-23.

Fischer, H. B., E. J. List, R. C. Y. Koh, J. Imberger, H. Brooks (1979), Mixing in inland and coastal waters, Academic Press, Inc.: New York, N.Y.

Fofonoff, N. P. and R. C. Millard (1983), Algorithms for computations of fundamental properties of seawater. UNESCO Technical Papers in Marine Science, No. 44, 53 pp.

French-McCay, D. P., C. Mueller, K. Jayko, B. Longval, M. Schroeder, J. R. Payne, E. Terrill, M. Carter, M. Otero, S. Y. Kim, W. Nordhausen, M. Lampinen, C. Ohlmann (2007), Evaluation of Field-Collected Data Measuring Fluorescein Dye Movements and Dispersion for Dispersed Oil Transport Modeling, paper presented at the 30th Arctic and Marine Oil Spill Program (AMOP). Technical Seminar, Emergencies Science Division, Environment Canada, Ottawa, ON, Canada.

Garrett, C. and W. Munk (1979), Internal waves in the ocean, *Ann. Rev. Fluid Mech*, 11, 339–369.

Geyer, W. R., A. Lavery, M. Scully, J. Trowbridge (2010), Mixing by shear instability at high Reynolds number, *Geophys. Res. Lett.*, 37, L22607.

Hendriks, T., and N. Christensen (1987), Current flow patterns in the San Diego Bight, annual report, pp. 27-31, *South. Calif. Water Res. Proj*., Westminster.

Hunt, C. D., A. D. Mansfield, M. J. Mickelson, C. S. Albro, W. R. Geyer, P. J. W. Roberts (2010), Plume tracking and dilution of effluent from the Boston sewage outfall, *Mar. Env. Res*., 70, 150–161.

Jones, B. H., A. Bratkovich, T. Dickey, G. Kleppel, A. Steele, R. Iturriaga, I. Haydock (1990), Variability of physical, chemical, and biological parameters in the vicinity of an ocean outfall plume, presented at the Third Int. Symp. on Stratified Flows, E. J. List and H. H. Jirka (eds.), ASCE, New York.

Jones, B. H., L., Washburn, Y. Wu (1991), The dispersion of ocean outfall plumes: physical and biological dynamics, presented at Coastal Zone '91, Proc. of 7th Symposium on Coastal & Ocean Management. ASCE, Long Beach, CA.

Jones, B. H., T. D. Dickey, L. Washburn, D. Manov (1993), Physical and biological dynamics of sewage outfall plumes in the coastal region: an integrated observational approach, Water Pollution 11: Modelling, Measuring, and Prediction, L.C. Wrobel and C.A. Brebbia (eds.), Computational Mechanics Publications, Southhampton. 527-534.

Koh, R. C. Y. and N. H. Brooks (1975), Fluid mechanics of waste water disposal in the ocean, *Ann. Rev. Fluid Mech*., 7, 187-211.

Lennert-Cody C. E., P. J. S. Franks (1999), Plankton patchiness in high-frequency internal waves, *Mar. Ecol. Prog. Ser*., 186, 59 – 66.

Mack, S. A. and H. C. Schoeberlein (2004), Richardson number and ocean mixing: Towed chain observations, *J. Phys. Oceanogr*., 34, 736–754.

Millero, F. J. and A. Poisson. (1981), International one-atmosphere equation of state of seawater, *Deep-Sea Res*., 28, 625-629.

Okubo, A., (1971), Oceanic diffusion diagrams, *Deep-Sea Res*., 18, 789-802.

Petrenko, A. A., B. H. Jones, T. D. Dickey (1998), Shape and initial dilution of Sand Island, Hawaii sewage plume, *J. Hydraulic Eng*., ASCE, 124, 565-571.

Petrenko, A. A., B. H. Jones, T. D. Dickey, M. LeHaitre, C. Moore (1997), Effects of a sewage plume on the biology, optical characteristics, and particle size distributions of coastal waters, *J. Geo. Phys. Res*., 102, 25061 - 25071.

Petrenko, A.A., B. H. Jones, T. D. Dickey, P. Hamilton (2000), Internal tide effects on a sewage plume at Sand Island, Hawaii, *Continental Shelf Res*., 20, 1–13.

Phillips, O. M., (1997), The Dynamics of the Upper Ocean, 2nd ed. London: Cambridge University Press.

Pineda, J., (1994), Internal tidal bores in the nearshore: Warm-water fronts, seaward gravity currents and the onshore transport of neustonic larvae, *J. Mar. Res*., 52, 427–458

Proni, J. R., H. Huang, W. P. Dammann (1994), Initial dilution of southeast Florida ocean outfall, *J. Hydraulic Eng*., ASCE, 120, 1409-1425.

Ramos, P., M. V. Neves, F. L. Pereira, I. Quintaneiro (2002), Mapping the Aveiro sea outfall plume: sampling strategy for an Autonomous Underwater Vehicle, presented at 2nd International Conference on Marine Waste Water Discharges, MWWD 2002, Istanbul, Turkey.

Ramos, P., S. R. Cunha, M. V. Neves, F. L. Pereira, I. Quintaneiro (2005), Sewage Outfall Plume Dispersion Observations with an Autonomous Underwater Vehicle, *Water Science and Techn.*, 52, 12.

Roberts, P. J. W. (1977), Dispersion of buoyant waste water discharged from outfall diffusers of finite length, thesis, presented to California Institute of Technology, at Pasadena, Calif., in partial fulfillment of the requirements for the degree of Doctor of Philosophy.

Roberts, P. J. W., W. H. Snyder, D. J. Baumgartner (1989), Ocean Outfalls. Parts I, II, and III. *J. Hydraulic Eng*., ASCE, 1–70.

Roberts, P. J. W. (1999a), Modeling Mamala Bay Outfall Plumes. I: Near Field, *J. of Hydraulic Eng*., ASCE. 125, 6, 564-573.

Roberts, P. J. W. (1999b), Modeling Mamala Bay Outfall Plumes. II: Far Field, *J. of Hydraulic Eng*., ASCE 125, 6, 574-583.

Roughan, M., E. J. Terrill, J. L. Largier, M. P. Otero (2005), Observations of divergence and upwelling around Point Loma, California, *J. Geophys. Res.*, 110, C04011.

Schmitt, R. W., R. C. Millard, J. M. Toole, W. D. Wellwood (2005), A double-diffusive interface tank for dynamic-response studies, *J. of Mar. Res.*, 63, 263-289.

Taylor, G. I. (1953), Dispersion of soluble matter in solvent flowing slowly through a tube, *Proc. R. Soc. Lond*., A219, 186-203.

Taylor, G. I. (1954), The dispersion of matter in turbulent flow through a pipe, *Proc. R. Soc. Lond*., 223, 446-468.

Terrill, E. (2009), IBWC Final Report - Coastal observations and monitoring in South Bay San Diego IBWC / Surfrider Consent Decree, February 25, 2009.

Thorpe, S. A., (1975), The excitation, dissipation and interaction of internal waves in the deep ocean, *J. Geophys. Res.*, 80**,** 328–338.

Tian, X., P. J. W. Roberts, G. J. Davero (2004), Marine Wastewater Discharges from Multport Diffusers II: Unstratifield Flowing Water, *J. of Hydraulic Eng*., 130, 12, 1147-1155.

Washburn, L., B. H, Jones, A. Bratkovich, T. D. Dickey, M. Chen (1992), Mixing, dispersion, and resuspension in vicinity of ocean wastewater plume, *J. of Hydraulic Eng*., ASCE, 118(1), 38-58.

Winant, C. D., A. W. Bratkovich (1981), Temperature and currents on the southern california shelf: a description of the variability, *J. Phys. Oceanogr.*, 11, 71–86.

Wu, Y. C., L. Washburn, B. H. Jones (1994), Buoyant plume dispersion in a coastal environment-evolving plume structure and dynamics, *Continental Shelf Res*., 14, 1001-1.